Master of Science Thesis

Ultrasonic Plastic Welding of Dissimilar Materials

Experimental investigation of metal/carbon fiber reinforced thermoplastic joints

Umberto Federico Dal Conte

15th December 2017

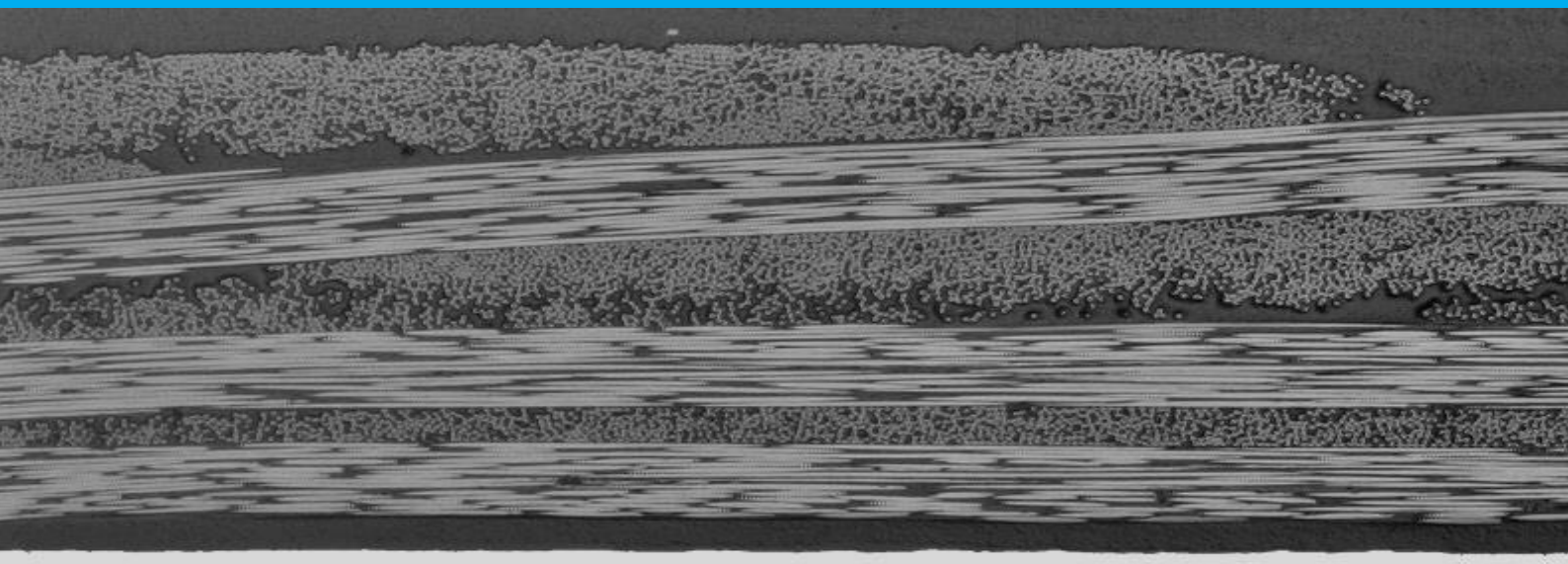

TU Delft Delft University of Technology

TOYOTA

Challenge the future

Ultrasonic Plastic Welding of Dissimilar Materials

Experimental investigation of metal/carbon fiber reinforced thermoplastic joints

Master of Science Thesis

For obtaining the degree of Master of Science in Materials Engineering and Applications at Delft University of Technology

Umberto Federico Dal Conte

15th December 2017

Faculty of Mechanical, Maritime and Materials Engineering · Delft University of Technology

Delft University Of Technology
Department Of
Material Science and Engineering

Dated: 15th December 2017

Head of department: _____
Prof. dr. ir. I. Richardson

Supervisor TU Delft: _____
Dr. ir. I. F. Villegas

Supervisor Toyota Motor Europe: _____
Ir. J. Tachon

Reader: _____
Dr. ir. S. Teixeira de Freitas

Abstract

Due to EU regulations on fuel consumption, reducing the weight of vehicles has become one of the most important goals of car manufacturers in Europe. Among them, Toyota Motor Europe is one of the worldwide leaders in the research for a sustainable future. Materials like fiber-reinforced plastics and aluminum play a significant role in the research for lightweight design, thanks to their very good strength-to-weight ratio. However, joining these materials efficiently together is still a challenge. When thermoplastic composites are used, direct joining with the metal substrate can be obtained using welding technologies which melts the thermoplastic at the interface.

Ultrasonic welding is well-known for being a fast, reliable and effective technology for metal/metal or plastic/plastic joining. In this study, a collaboration between Toyota and TU Delft, ultrasonic plastic welding was investigated as candidate joining technology for aluminum/thermoplastic joints in automotive applications. The goal was to understand the main mechanisms involved in the adhesion and how they affect the performance of the joint. Initially, the technique proved to be successful, but moderate strengths were obtained. Therefore, several surface pre-treatments of the aluminum were analyzed to improve performance in terms of strength and durability of the joint; mechanical, chemical and physical treatments were carried out. With laser structuring, strengths comparable to adhesive bonded joints were obtained, but in a much shorter process time. Other treatments such as conversion coating, sandblasting and plasma led to considerable improvements as well.

The encouraging results achieved represent an important step in the development of ultrasonic plastic welding for multi-material joining in the automotive industry. Additional research could help Toyota and other car manufacturers realizing a better design to further decrease weight and CO_2 emissions of vehicles.

Acknowledgements

This final report represents the end of two amazing years spent in the Netherlands, a country who welcomed and hosted me in the best way I could possibly imagine. All the people I met along this journey helped me grow from both a personal and an academic point of view, and I will always be grateful to them. In particular, I wish to thank Irene, my thesis supervisor in Delft, who was always able to transmit enthusiasm and passion for the work I was doing; I am thankful for everything I learned from her and from the whole welding group: Bram, Eirini, Genevieve, Nikos and Tian. I would like to thank also all the professors and academic staff for their expertise and their availability.

Then, none of this project would have been possible without my company supervisor, Julien. Since my internship in Toyota, he has always been a true source of inspiration, showing me to never settle and guiding me along my path. It was a pleasure for me working with him and with Toyota.

A special "grazie" goes to the amazing people who shared these two years with me in Delft. I will always keep our memories deep in my heart and I will miss so much: Ale, Anto, Cami, Davide, Edo, Fede, Fede Trova, Gigi, Giulia, Greta, Hans, Luca, Lu ♡, Matte, Mitro, Olto and Simo. I hope I left you at least one tenth of what you gave me.

If I am here today, it is only thanks to my beautiful family, who was by my side in every important decision in my life and always supported and encouraged me. Papà e Mamma, I am so proud to be your son, you are the best parents someone could have. Ire, you are a wonderful sister and I will always love you. Nonni, zii e cugini, thank you for always being there when I needed it.

Last but definitely not least, the ultimate thanks goes to my second family, because that is who you are to me: the people I shared the best and worst moments of my life with, the people I can always count on and the people that made me who I am. Ali, Baudo, Dodo, Ema, Ludo, Marco, Marta, Romans, Ste, Zaf, Ludone, Ale, Bila e Drea, words will never express what you really mean to me.

15th December 2017 *Umberto Federico Dal Conte*
Delft, The Netherlands

Contents

List of Figures

List of Tables

Chapter 1

Introduction

1.1 Motivation

In the automotive industry, the development and use of lightweight materials are largely growing in order to reduce CO_2 emissions. EU legislation set mandatory emission reduction targets for car manufacturers, whose goal is to obtain a fleet average of 95 grams of CO_2 per kilometer by 2021. As a result, materials like aluminum and fiber-reinforced plastics (FRPs) are finding new ways of employment (Fig 1.1, 1.2) thanks to their high strength-to-weight ratio. Toyota Motor Corporation (TMC), the world's second largest automobile manufacturer by production and the leader in hybrid vehicles sales, has always promoted research and technology for a sustainable, low-carbon society. Toyota Motor Europe (TME) with its Lightweight Team in Material Engineering Division is working steadily to help accomplish these goals. However, in order to fully take advantage of specific material properties, effective multi-material joining technologies need to be established: the intrinsic differences in physical and chemical properties create significant challenges in the joint design.

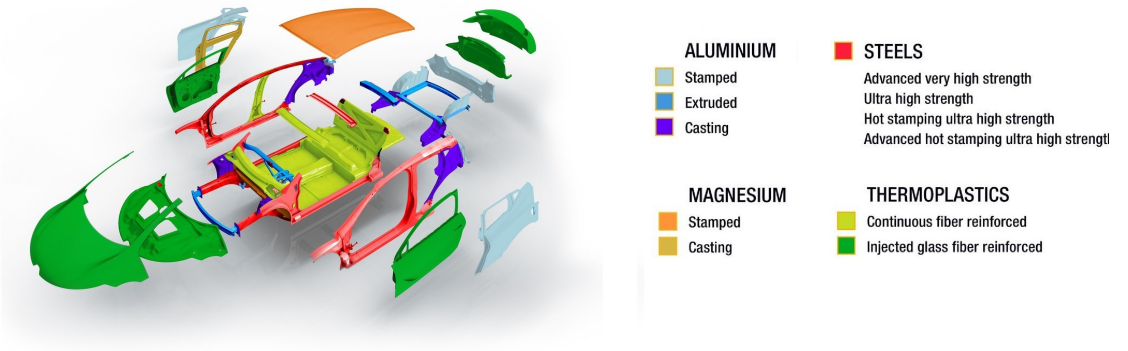

Figure 1.1: *Eolab concept by Renault for an ultra-light car made from steel, aluminum, magnesium and composites*

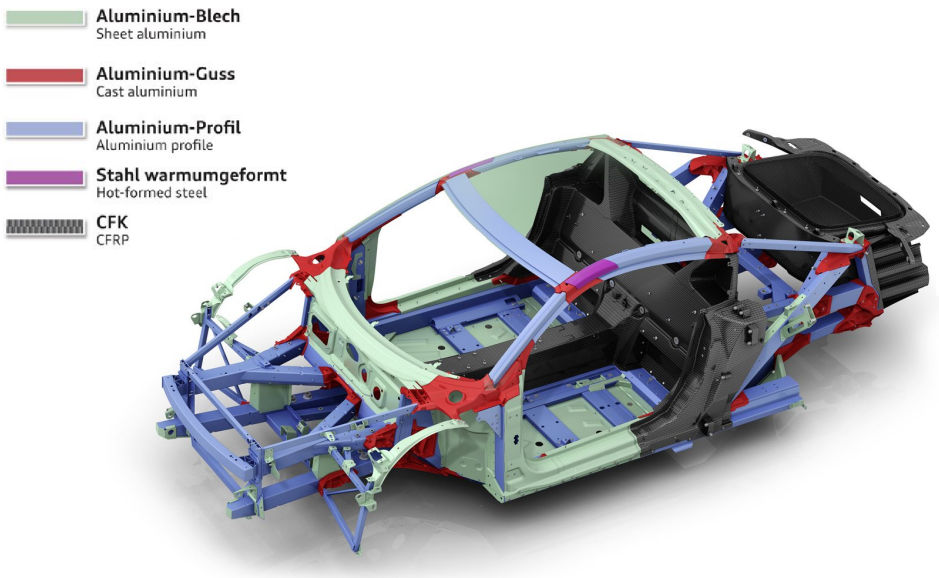

Figure 1.2: *Audi Multi-material Space Frame concept applied to the R8 e-tron model*

Current common methods are mainly based on mechanical fastening and adhesive bonding, because of the large experience acquired in the last decades. Both have their own advantages and limitations, which can be summarized as follows.

Mechanical Fastening

Mechanical fastening is used when component disassembly is necessary, failure is relatively easy to predict and installation requires little technology. Conversely, fastenings produce stress concentrations, galvanic corrosion between the fastener and the component can occur, it is labor intensive and obviously there is a considerable increase in weight.

Adhesive Bonding

Adhesive bonding distributes the load over a large surface leading to more uniform stress along the overlap area. Good fatigue resistance is obtained, sealing is ensured and since no fastener is used there is large weight reduction; however, it requires long processing times due to extensive surface preparation of the adherends and curing of adhesives, potential thermal and environmental degradation of the adhesive can take place, disassembly is not possible and extra care on human safety and environment needs to be taken.

Welding

In light of the above, new ways of direct joining are sought. A third well-known joining technique is welding or fusion bonding. Among FRPs, thermoplastics are the ideal choice for welding since they can be re-melted. As a result, several welding technologies are

emerging which are able to bond metals directly to thermoplastics, offering new and encouraging solutions for the future.

1.2 Objective

In this project, a collaboration between TU Delft and Toyota Motor Europe, ultrasonic plastic welding is investigated as a candidate joining technology for automotive applications. The objective is to understand and analyze the joining process between carbon fiber reinforced thermoplastic and metal, focusing on the main factors affecting adhesion, strength and durability.

Research Questions

This objective can be structured in the following research questions:

1. What is the melting behavior of the thermoplastic during the welding process and how does it affect the adhesion between CFRP and metal?
2. What is the initial strength of the joint and how does it compare to other joining techniques used in automotive?
3. Based on the adhesion mechanisms, how is it possible to increase joint strength?
4. What are the effects of temperature and moisture on adhesion and on the joint performance?

In this study, these points were analyzed and discussed with an experimental approach, in order to explore new solutions and to expand current knowledge on this technology.

Chapter 2

Literature Review

In Chapter 1, it was mentioned that fusion bonding is an appealing technology for joining metal to thermoplastics. In this chapter, a brief overview of current welding technologies is given, focusing on ultrasonic welding; besides, a review on different ways of improving joint performance by surface treatments of the metal is carried out, along with a short analysis on the durability of metal/thermoplastic joints.

2.1 Welding Technologies

Even though there are many different welding technologies involving direct metal/polymer bonding (Fig. 2.1), all share the same working principles: the polymer at the interface is brought to a viscous state by heat and the two surfaces into intimate contact, followed by cooling under pressure for consolidation [1, 2].

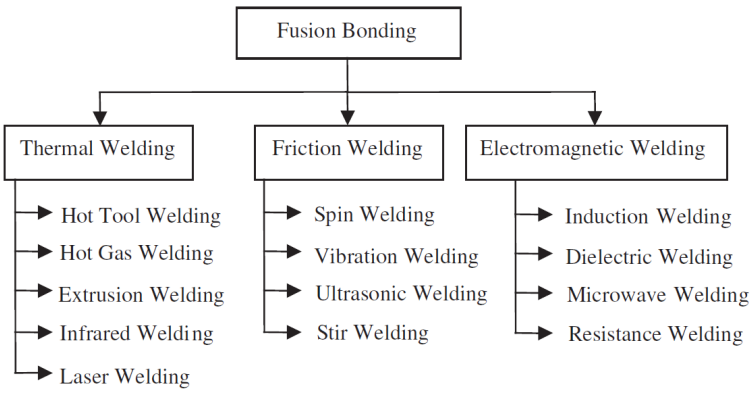

Figure 2.1: *List of available welding technologies based on heating principle [3]*

Direct adhesion between the metal surface and the thermoplastic matrix occurs. A first essential requirement for proper adhesion is good wetting of the surface, which depends on

the relative surface energy of the two substrates. Adhesion phenomena are typically represented by the following theories: mechanical interlocking model, adsorption, electrostatic theory, interdiffusion, weak boundary layer theory and chemical bonding [4]. Despite chemical bonds being the strongest bonds existing, thermoplastics are usually chemically inert so the latter theory is not expected to be applicable. Mechanical interlocking and adsorption are therefore believed to have the biggest influence on joint strength [5, 6]. Mechanical interlocking originates from the molten polymer which spreads into the metal surface asperities. Adsorption is based on a physical interaction between the two materials, where hydrogen and Van der Waals bonds are formed at the interface (Fig. 2.2).

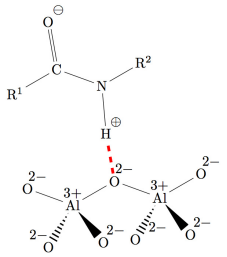

Figure 2.2: *Example of hydrogen bond between Nylon and Aluminum [7]*

Ultrasonic Welding

Among all different welding technologies, ultrasonic welding was chosen for this research because of its very promising features: extremely fast process times, medium-to-high strengths, good reproducibility, low energy input and the possibility of automation [8].

The technique uses ultrasonic vibration to introduce heat at the interface and allows bonding to occur. It can be divided into ultrasonic metal welding (UMW) and ultrasonic plastic welding (UPW). They share almost the same working characteristics, the only difference is the direction of the ultrasonic oscillation: in case of UMW the oscillation is parallel to the welding surface, while in UPW the oscillation acts perpendicular to the welding surface (Fig. 2.3).

The main components of an ultrasonic spot welding equipment are the following: an ultrasonic generator converts standard voltage to high frequency alternate voltage. The converter transforms the voltage into mechanical oscillation thanks to the piezoelectric effect. The correct oscillation is then reached in a booster and transmitted to the joining partners through a sonotrode, which presses the material against an anvil in order to achieve a certain welding pressure.

The ultrasonic welding process mainly consists of a vibration phase followed by a solidification phase. The main process parameters are the oscillation amplitude, the welding force and the welding energy but also material parameters like topography, geometry and physical properties affect the final result. The influence of each parameter for UPW was studied by Villegas et al. [2] [9]. Instead of welding energy, sonotrode displacement has been successfully used to control the process [5, 9].

Compared to UMW, UPW has the main advantage of shorter welding times, which is very important for the automotive industry. Common practice with UPW and thermoplastic

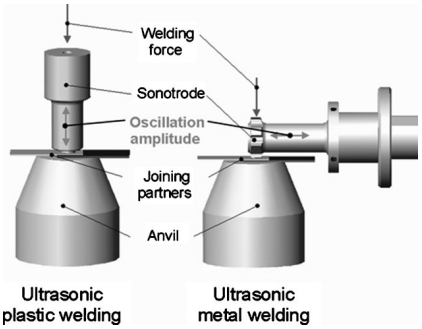

Figure 2.3: *Difference setup between UPW and UMW [10]*

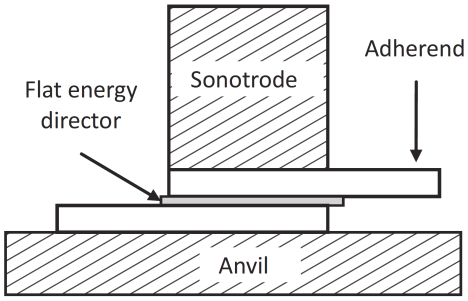

Figure 2.4: *Schematic of the UPW process with flat energy director [11]*

composites is the use of so-called energy directors (EDs). These can be either some shaped protuberance or flat films at the interface between the two joining partners (Fig. 2.4): they consist only of polymeric material which experiences larger strain than bulk material because of the lower elastic modulus [11], leading to preferential melting at the interface. In order to optimize the process and obtain good consistent weld quality, the interaction of amplitude and welding pressure with sonotrode displacement and dissipated power was investigated for CF/PEI and flat EDs [9, 11]. Five welding stages in the vibration phase were identified (Fig. 2.5):

- Stage 1 - increase in dissipated power due to heating of the energy director
- Stage 2 - power decrease with constant sonotrode displacement, indicating local melting of energy director
- Stage 3 - sonotrode starts moving downwards with an increase in power, with the fully molten energy director that starts flowing
- Stage 4 - matrix in the bulk material starts melting together with energy director flow, thus a plateau in the dissipated power is present
- Stage 5 - melting of the matrix is predominant, characterized by a drop in power

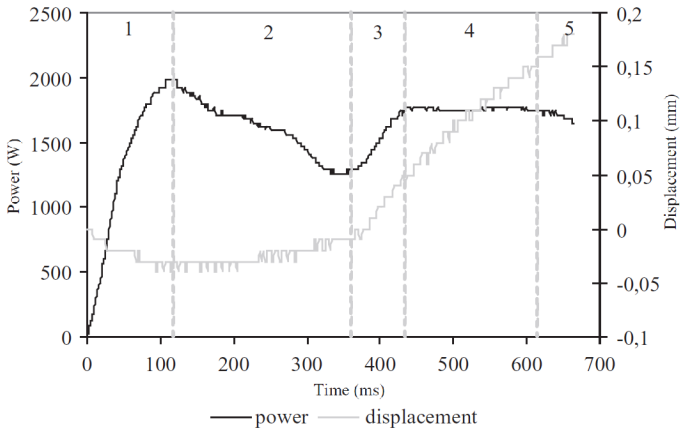

Figure 2.5: *Schematic of the stages in the vibration phase of UPW [9]*

In the work of Bolt [5] on welding CF/PA6 to aluminum and steel, the previously mentioned welding stages could not be fully recognized; thus, it was not possible to quickly identify the ideal set of parameters. Additionally, metal substrates had to be coated with thermoplastic film in order to guarantee a bond with the CFRP and to preserve the surface when some pre-treatments were applied. These pre-treatments were tested to increase the joint strength, as can be seen in Figure 2.6.

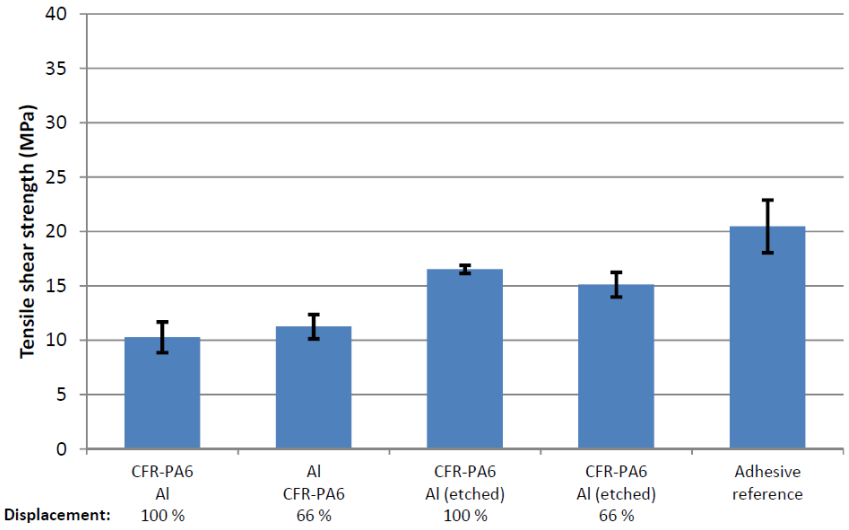

Figure 2.6: *Lap shear strength of welds created by Bolt with different metal surface treatments [5]*

Other Technologies

Other welding methods for metal-thermoplastic direct joining were examined as well in order to determine similarities and differences and to gain some knowledge on the factors affecting adhesion. Resistance welding [12, 13], induction welding [14–16], friction spot joining [6, 17] and laser welding [18–22] were considered. All techniques confirm that adhesion is based mostly on mechanical interlocking and physical forces between the adherends. Most of the literature pointed out the need of some surface pre-treatment of the metal substrate to considerably improve the joint strength; these treatments range from simple sandblasting to complex electrochemical processes like anodizing.

2.2 Influence of Surface Pre-treatments of Metals on Adhesion

In general, the main goals of surface pre-treatments can be summarized as follows: to remove contaminants and other weak layers; to improve adsorption and wettability of the surface; to increase roughness and bonding area; to promote formation of physical and chemical bonds; to improve corrosion resistance. Treatments for metals can be divided in mechanical, chemical or physical treatments. No treatments of the thermoplastic were investigated since the composite melts during the welding process.

2.2.1 Mechanical Treatments

Mechanical treatments are mainly aimed to increase contact surface and therefore to enhance mechanical interlocking. Techniques include sandblasting, laser ablation and structuring [23–28] or production of through-thickness reinforcements in order to increase peel strength as well [29–35].

2.2.2 Chemical Treatments

Chemical treatments usually aim to enhance surface properties by either eliminating any kind of contamination, by micro-roughening the surface or by adding corrosion resistant layers. In traditional procedures for aluminum, usually the first step is solvent degreasing followed by a more aggressive cleaning (deoxidizing/etching) by alkaline rinse, acid rinse and water rinse [36]. In addition, procedures involving anodizing or conversion coatings can be applied [37].

2.2.3 Physical Treatments

Physical treatments are used when cleaning and activation of the surface are required, in order to increase surface tension and improve adhesion in materials that exhibit bad wetting behavior. A common example is plasma treatment [38, 39]: this can be used for reduction of metal oxides, ultra-fine surface cleaning from organic contaminants or deposition of functional chemical groups, with the advantage of a fast and environmentally safe process compared to wet chemical treatments.

2.3 Durability of Metal/Thermoplastic Joints

One of the most important requirements of joints is to guarantee long-term performances; this is particularly true for multi-material joints, as different mechanisms may cause degradation of the joint in the presence of moisture (Fig. 2.7, 2.8) or higher temperatures [40–43].

First and most important, degradation of the interface can occur: loss of adhesion is caused by chemical interaction between the OH groups of the polymer and water molecules, which breaks hydrogen bonds and displace OH groups away from the surface [44].

Second, thermoplastics can absorb water which weakens the material by swelling, plasticization or formation of micro-cavities [40, 43, 44]; however, many of these effects are reversible by drying the thermoplastic.

Third, when dissimilar electroconductive materials are in contact, galvanic corrosion prevention is of primary importance. In the work of Bolt [5], electro-insulation of hybrid welds created by ultrasonic plastic welding was tested in order to verify weather galvanic corrosion between metals and CFRP can be avoided. It was found that the thermoplastic layer between carbon fibers and metal allows achievement of electrical insulation, thus

galvanic corrosion is highly decreased and does not represent a substantial issue in case of ultrasonic plastic welding.

Finally, depending on the corrosion resistance of the chosen material, oxidation of the metal surface is a possibility, along with metal hydration which forms a mechanically weak layer at the interface [40, 44].

Corrosion resistance and durability of multi-material joints can be improved by proper pre-treatments of the substrates: many examples can be found in the literature where higher mechanical interlocking or stronger bonds at the interface enhanced residual strength after artificial aging [8, 35, 40, 45, 46].

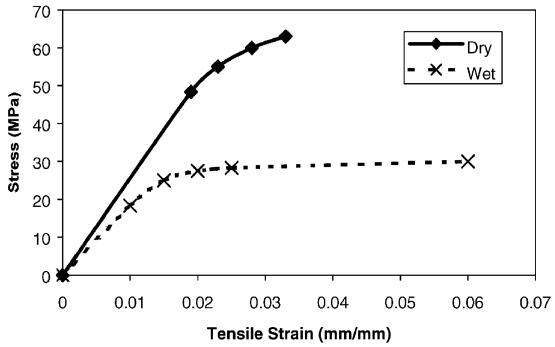

Figure 2.7: *Effect of moisture on the mechanical properties of adhesive joints [43]*

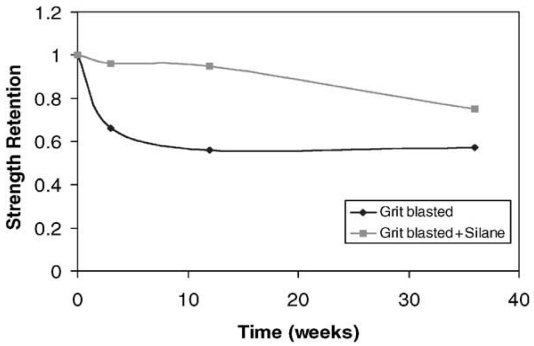

Figure 2.8: *Effect of water uptake on the joint strength (butt joint configuration) [43]*

2.4 Conclusion

Joining composites to metals is still a significant challenge in the automotive industry. When thermoplastics are used, ultrasonic welding seems a promising solution since it provides high quality welds in extremely short times.

Direct bonding between the substrates occurs, mainly due to mechanical interlocking and adsorption, the dominant adhesion mechanisms. In order to obtain stronger bonding, surface pre-treatments of the metal substrate were discussed, underlining their effects on the adhesion mechanisms.

Finally, long-term durability of the joint in automotive relevant conditions is a critical aspect to consider when designing a joint. Potential environmental degradation occurring in the joint was briefly presented, and the importance of pre-treatment in these cases was underlined as well.

Chapter 3

Experimental Set Up

The experimental work of this project can be divided into three main parts: welding without surface treatments of the metal adherend, welding with surface treatments of the metal adherend and testing durability of the welds (both with and without treatments). In the first part, the focus was primarily on the welding process itself and on the bonding mechanisms occurring between metal and CFRP. In the second part, improvement of joint performances was targeted. In the third part, the influence of temperature and moisture in the joint was evaluated.

3.1 Materials

Most of the materials used in the research were supplied by Toyota Motor Europe; adherend samples were cut to the required dimensions by waterjet and sent to Delft. The geometry studied was a single-lap joint. The study was initially expected for two types of metal and two types of CFRP (Tab. 3.1, Fig. 3.1). However, after the first trials, welding of steel resulted in technical and experimental problems (see Appendix B), not beneficial to the goal of the project. Thus, only welding with aluminum is analyzed, with a higher focus on the combination with CFRP_1 since the material combination was closer to the current knowledge on ultrasonic plastic welding in TU Delft.

3.1.1 Manufacturing of Energy Directors

For the energy director, three different films were tested throughout the research (see Appendix A). Initially, a PA6 film supplied by Kaiserslauten University was used, but eventually, transparent Akulon F136-E1 available in the lab was chosen for most of the welds. Since the Akulon film was very thin (0.12mm), a thicker film was manufactured stacking two layers of film and consolidating them using a JOOS hot press following the cycle shown in Figure 3.2, to obtain a total thickness of 0.24mm. A silicone rubber sheet was placed between the press plates and the ED to obtain more uniform pressure;

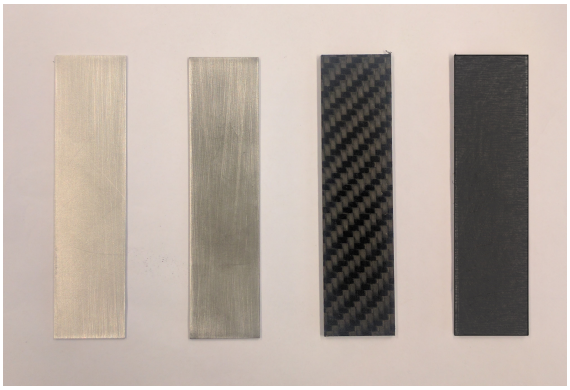

Figure 3.1: *Materials intended to be used in the study. From left to right: Aluminum, Steel, CFRP_1, CFRP_2. Steel was not investigated eventually. CFRP_2 appearance was modified for confidentiality*

Table 3.1: *Properties and characteristics of the materials employed in the research*

Material	**Characteristics**	**Size [mm]**	E **[GPa]**	σ_u **[MPa]**
Aluminum	6016 Ti-Zr coated	25x100x0.9	72	244
Steel	Zinc coated **Not investigated**	25x100x1	210	980
CFRP_1	CF/PA6 Woven fabric fibers	25x100x2	53	/
CFRP_2	CF/PA6 Confidential fiber distribution	25x100x2	<CFRP_1	/
Energy Director	PA6 film Akulon F136-E1	(thickness) 0.24	/	/

direct contact between silicone and ED was avoided by using a protective Kapton film in between. After the consolidation of the thicker ED film, squares of about 30 mm × 30 mm were cut, large enough to cover the whole overlap area.

PA6 is well known for being hygroscopic: to avoid unwanted moisture in the materials, all EDs and CFRP samples were dried at 110°C for at least 16h in vacuum using a Heraeus Vacutherm oven before welding, and kept in a desiccator if needed for further analysis.

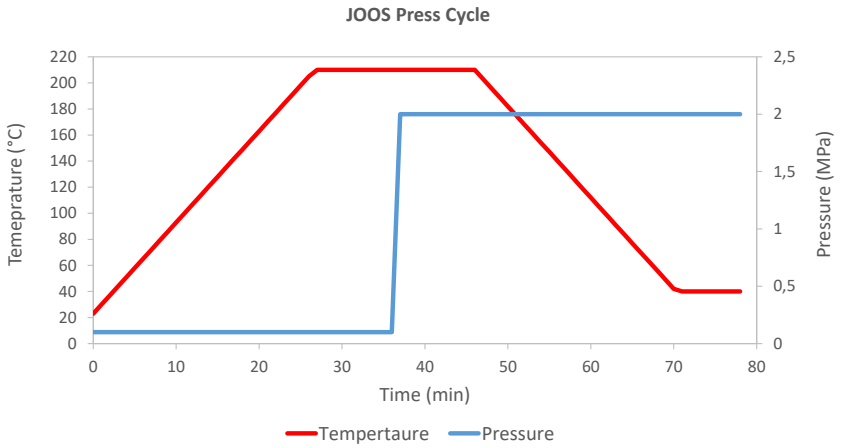

Figure 3.2: *Temperature and pressure cycle used to fabricate EDs with hot press. Heating and cooling rate were 7 °C/min*

3.2 Methods

In this section, a description of how welds were produced and analyzed is given. In order to understand how bonding occurred, both the interface and the joint performance were examined by different techniques.

3.2.1 Welding Process

Welding was performed using a Rinco 3000 ultrasonic plastic welder, which provides 20kHz and maximum power of 3000W, with a round titanium sonotrode (⌀=40mm). For specimen clamping, a jig designed with the purpose of obtaining constant overlap area of 12.7 mm × 25 mm conforming to ASTM D1002-05 was used. The jig also prevents shifting of the two substrates and thanks to a sliding platform, it allows for vertical movement of the top substrate to minimize bending (Fig. 3.3).

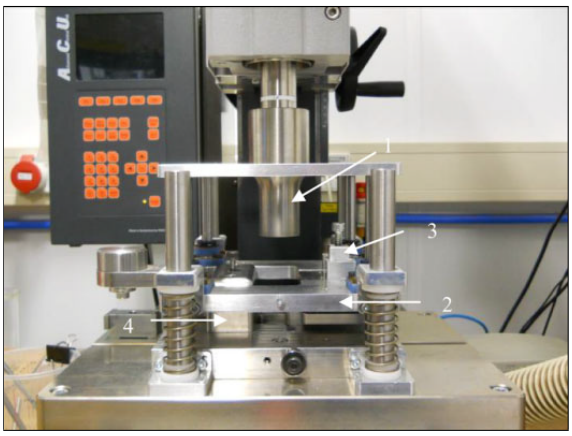

Figure 3.3: *Ultrasonic plastic welder and clamping jig: 1) sonotrode 2) sliding platform 3) upper clamp for top substrate 4) lower clamp for bottom substrate [9]*

In order to have a suitable reference for future developments, a fixed welding pressure and welding amplitude were chosen. After some trials (see Appendix C) and based on literature, welding force was set to 500N ($\approx$ 1.5 MPa) and semi-amplitude to 34.5 µm. These ensure enough contact between the substrates without damaging the metal: if amplitude was higher, cracks at the edge of the overlap were found in the aluminum (Fig. 3.4) when this was the top adherend. The process was controlled by sonotrode displacement, which was set to 100% of the ED thickness; after the vibration phase, a consolidation time of 4 seconds and 500N were applied. During welding, power, displacement, energy and time were recorded and the corresponding power-displacement curves were used to interpret changes occurring at the interface.

As explained in better details in Chapter 4, both welding with the aluminum as top adherend and bottom adherend was tested. This was done in the interests of providing complete information to the research and, from an industrial perspective, to assess weldability from both sides of the joint.

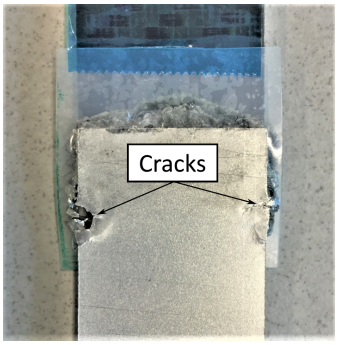

Figure 3.4: *Cracks at the edge of the aluminum if the amplitude is too high*

Figure 3.5: *Adhesive reference joint with Aluminum and CFRP_1*

3.2.2 Adhesive Reference

To properly judge the weld performances, it was important to compare it with other common techniques used in the automotive industry for multi-material joining. In this case, adhesive bonding was chosen as the reference technology. The adhesive used was epoxy Betamate 1822, supplied by Dow Automotive. Both metal and CFRP samples were only degreased before bonding and glass beads between 200 µm and 300 µm were used to control the bondline thickness. The adhesive was applied over an area with the same dimensions as the welded joints (12.7 mm $\times$ 25 mm), leaving spew fillets at the edges of the overlap (Fig. 3.5). Small clamps were used to apply some pressure. The joints were then put in a Votsch VTU oven at 180°C for 30 minutes to allow the adhesive to cure, following the supplier's instructions.

3.2.3 Temperature Measurement

In all welding processes, temperature is an important parameter to be determined since many physical and chemical transformations are temperature dependent. However, mea-

suring the temperature at the interface in ultrasonic plastic welding can be problematic: the overlap area is not easily accessible for infrared measuring and placing thermocouples directly between the substrates can alter the process because they act as energy directors. To overcome this problem, thermocouples type K (∅=0.1mm) were embedded into the EDs. In this case, Kaiserslauten PA6 was used (see Appendix A), with the same hot press procedure as ED fabrication but using 4 layers of film (total thickness=0.36mm) and the thermocouple in the middle (Fig. 3.6): the purpose was to have the thermocouple tip in the center of the overlap. Then the thermocouple output was recorded using a 10 Hz Pico TC-08 Thermocouple Data Logger, which compares temperature and time.

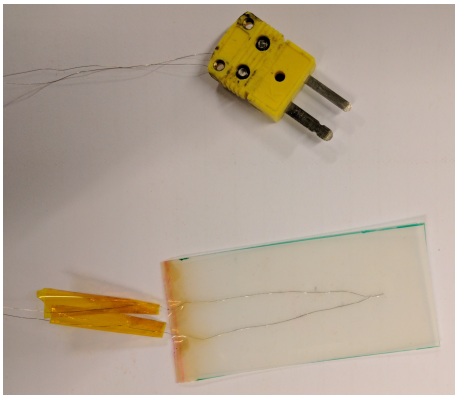

Figure 3.6: *Thermocouple embedded in the energy director*

A second way to measure the temperature during the process was carried out as well. A hole of ∅=0.5mm was drilled in the metal, 4mm deep in the middle of the overlap (Fig. 3.7). The same type of thermocouple as before was then inserted into the hole and fixed with polyamide tape to ensure that the it could not slip out during the welding process. It was then connected to a 100 Hz thermocouple input module (National Instruments 9213), in turn connected to a CompactDAQ Chassis (cDAQ-9178); measurements were finally recorded using a template code for thermocouples acquisition signal in LabView 2017.

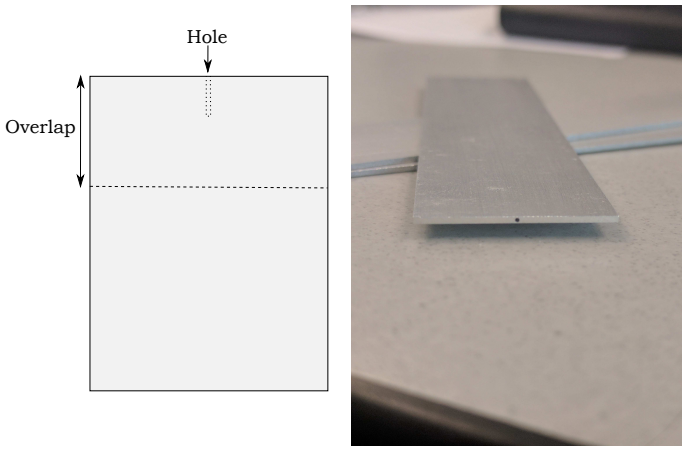

Figure 3.7: *Hole in the aluminum to place the thermocouple to measure temperature in the overlap*

3.2.4 Mechanical Testing

Mechanical tests were performed according to ASTM D1002-05 standard using a Zwick 10kN tensile testing device (Fig. 3.8). When needed, additional tabs where used in order to align the weld to the applied load.

A grip-to-grip separation of 130mm was set to fully cover the grips and a testing speed of 1.3mm/minute until joint failure was set. A small preload of 10N was also set to guarantee tensile stresses in the joint at the beginning of the test. Usually a minimum of four specimens was tested for each kind of weld; however, in a few cases, this number was reduced to 3 specimens due to lack of material available.

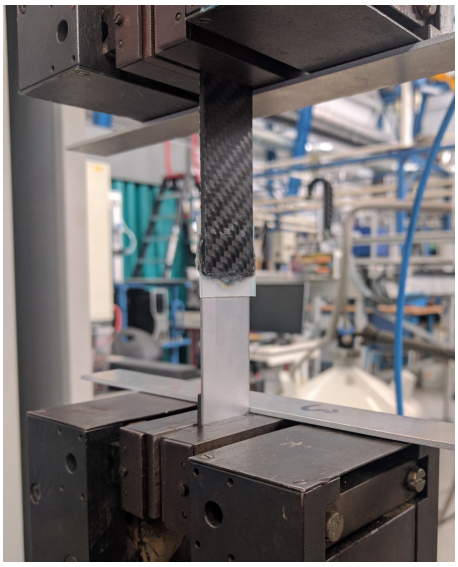

Figure 3.8: *Lap shear test setup*

3.2.5 Microscopy

Samples for interface observation were cut, embedded in epoxy resin, ground and polished with a Struers automated polisher. An optical microscope KEYENCE was employed with magnification up to 5000 (Fig. 3.9). In some cases, this microscope was also used to do initial observations of fracture surfaces after joint failure. To grasp more detail of fracture mechanisms and to analyze the effects of the different metal treatments, SEM-EDS was employed for surface analysis, before and after joining; the equipment used was a JEOL JSM-7500F Field Emission Scanning Electron Microscope. Thermoplastic samples were gold sputtered before observations to avoid charging. Finally, to obtain a quantitative evaluation of roughness for the different surface treatments, a Confocal Olympus Lex OLS3000 microscope was used: it allows investigation of an area of $256\,\mu m \times 192\,\mu m$, calculating the arithmetical mean height of the surface (R_a) and the root mean square height of the surface (R_q).

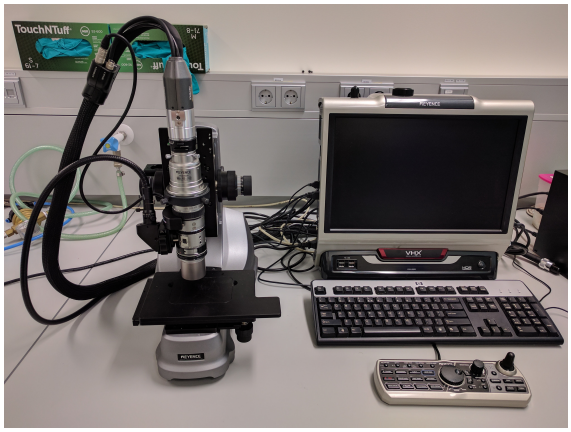

Figure 3.9: *Optical microscope used for investigating welded interface and fracture surfaces*

3.2.6 Surface Treatments

In the first part of the research, the metal substrates were only degreased with solvent HYSO QD. In the second part of the research different kinds of surface treatment were employed on the metal adherends, which are summarized in Table 3.2.

Table 3.2: *List of all planned surface treatments on the metal substrate*

Type	Description
Mechanical	Sandblasting
	Laser structured grooves
	3D-printed pins on existing Al substrate
	Metal hooks
Chemical	Alkaline and acid etching
	Acid pickling
	AMALPHA treatment
	Conversion Coating
Physical	Plasma

Sandblasting

Sandblasting was performed manually in TU Delft in a sandblast cabinet, using alumina particles between 0.35mm and 0.5mm. Particles were shot perpendicular to the surface from a distance of approximately 10cm for about 10 seconds.

Laser Structuring

In collaboration with a German research institute and Toyota, grooves could be created by laser on the aluminum samples. This allows the molten matrix to flow and fill the grooves, in order to enhance mechanical interlocking and therefore to increase the joint strength. Two different types of structuring were carried out by the institute (Tab. 3.3):

Table 3.3: *Laser modes characteristics*

Mode	Speed	Passes	Pitch distance	Groove depth	Power
Galvo Scanner	15 m/s	2	≈200 µm	≈75 µm	1kW
Polygon	25 m/s	7	≈300 µm	≈400 µm	2kW

With Galvo Scanner mode the grooves were supposed to have a traditional notch-rounded shape (Fig. 3.10); with Polygon mode, grooves were supposed to be deeper and with a drop shape to increase interlocking (Fig. 3.11).

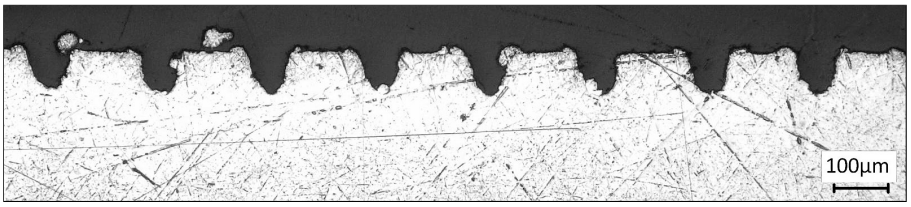

Figure 3.10: *Grooves produced by laser in Galvo Scanner mode*

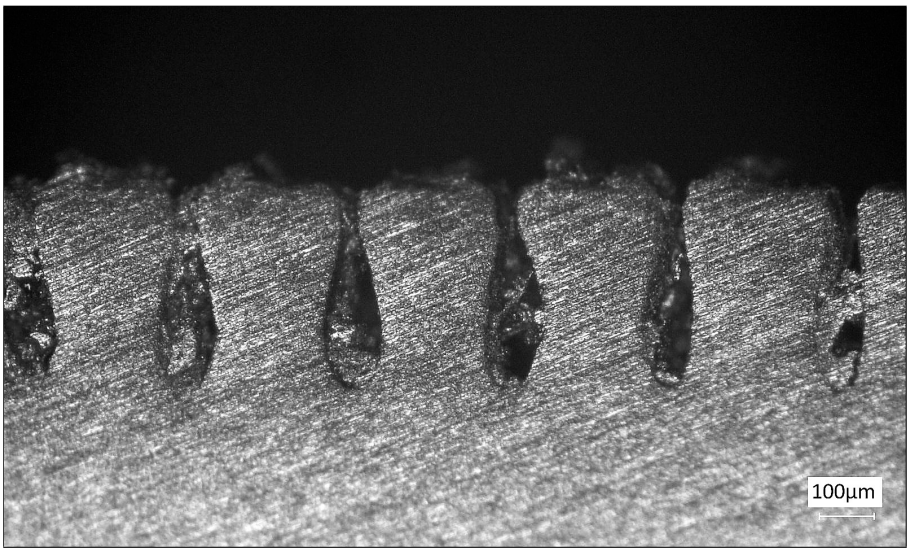

Figure 3.11: *Grooves produced by laser in Polygon mode*

3D Printing

With the help of JP3D-TecVision it was possible to print customized pins on existing aluminum samples, to attempt increasing both shear and peel strength of the joint. To optimize the process and bring it to a small series production level, a positioning mould (Fig. 3.12) was first created, where each sample could be easily placed for the subsequent treatment. The technology is based on selective laser melting (SLM) which uses high-power density laser to melt and join metallic powders together [47]. Eighteen pins were successfully printed on each sample (Fig. 3.13, 3.14). During welding, the displacement was always set to the pin height in order to guarantee that the pins would penetrate completely the thermoplastic substrate; besides, welding with and without energy director was tested to check potential differences.

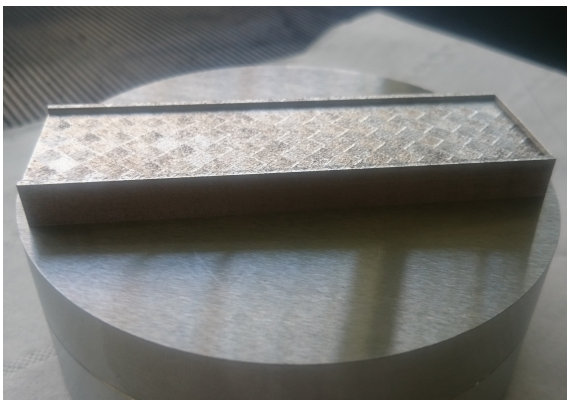

Figure 3.12: *Positioning mould for 3D printing*

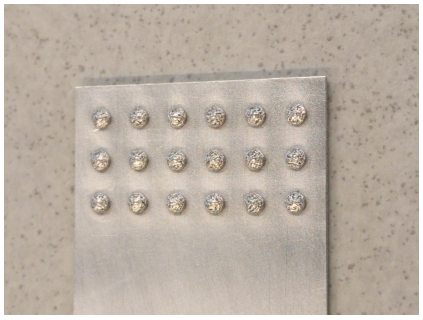

Figure 3.13: *3D printed pins on Al sample*

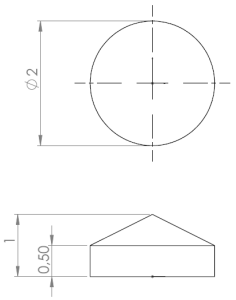

Figure 3.14: *Pin shape and dimensions used: ∅=2mm, height=1mm*

Metal Hooks

Another technology suitable to create through-thickness reinforcements has been developed in Canada: it applies an array of micro-formed hooks that can physically adhere with other materials without the use of traditional adhesives, according to the manufacturer (Fig. 3.15). A hook height of 1mm and a straight shape were chosen for this study. Also with this type of treatment, displacement was set to the hooks height and welding with and without energy director was tested.

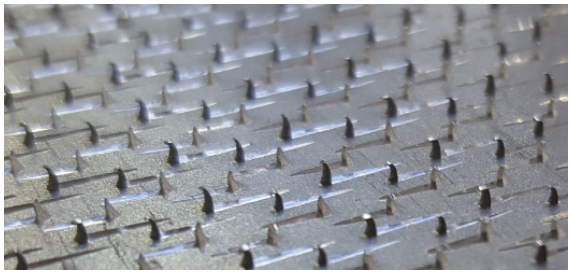

Figure 3.15: *Several hooks created on the Aluminum samples surface*

Etching and AMALPHA

Among chemical treatments, etching of aluminum is one of the most common in industry: it allows removal of the weak layers or the existing oxide layer and creation of a new, more stable oxide. For this project, three different etching procedures were tested.

Alkaline-acid etching is frequently used for aluminum treatment prior to adhesive bonding [37, 48]. Therefore, in the first chemical treatment, samples were first immersed in an alkaline NaOH solution for 15 minutes to dissolve any oxide on the surface; subsequently, they were rinsed with DI water and immersed in an acid solution with HNO_3 for 5 minutes to remove any deposit. Finally, they were rinsed again with DI water and dried with compressed air.

The second etching procedure was based on the work of Bolt [10]: the samples were immersed only in HNO_3 at 65% concentration (acid pickling) but for 15 minutes and then rinsed with DI water and dried with compressed air.

The third process was performed by an external company (MEC, Belgium) and it is called AMALPHA treatment. This was reported by the company and in literature [49] to be very effective for fusion bonding with thermoplastic due to increased microroughness for better interlocking, as can be seen in Figure 3.16. Several immersion times were tested by MEC in order to create higher or lower roughness.

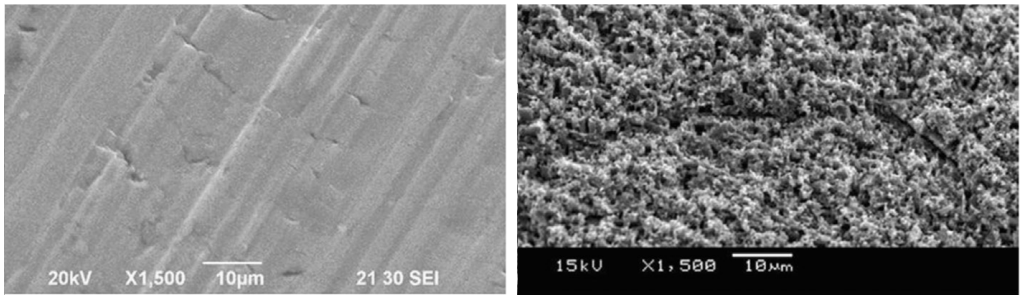

Figure 3.16: *Rougness difference of aluminum surface before (left) and after AMALPHA treatment (right) [49]*

Conversion Coating

Conversion coatings are good alternatives to more complex treatments like anodizing to improve the durability of an adhesive bond [50, 51]. BONDERITE M-NT 30002 by Henkel

was used, based on Cr^{3+} and Zr which forms two thin zirconium and chromium oxides. Samples were cleaned in an alkaline NaOH solution for about 30 seconds and then dipped in a solution with 3 vol% of BONDERITE M-NT 30002; the pH was controlled between 4 and 4.3 with an application time of 60s, followed by rinsing in DI water and drying with compressed air.

Plasma Treatment

Air plasma treatment was used, generated by a plasma system Tigres CKG-20 with a corona discharge gun; samples were placed on a support to bring the surface in contact with the plasma cloud (Fig. 3.17). A speed of 5mm/s was chosen with double passage per sample.

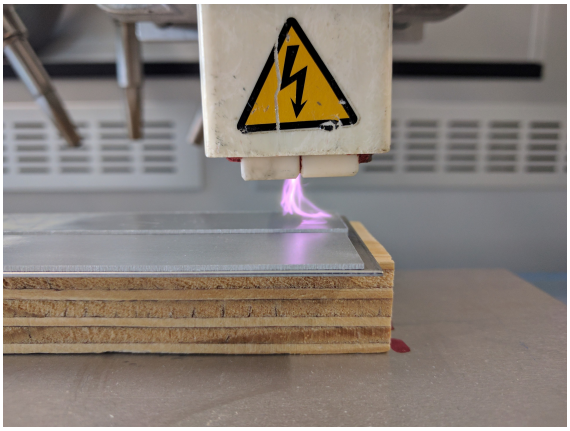

Figure 3.17: *Example of aluminum samples undergoing plasma treatment*

3.2.7 Durability: Artificial Accelerated Aging

In order to test different environmental conditions on the joint, two types of tests were carried out: the effects of moisture and temperature were targeted. Both tests were performed almost entirely in Toyota Motor Europe.

Moisture absorption

In the first test, the welds were immersed in DI water at 80°C for at least 24 hours. The test follows a Toyota standard procedure to bring the thermoplastic to moisture saturation. Based on previous experience in Toyota for similar joints, this test was expected to be quite aggressive in terms of interface degradation (see Sec. 2.3).

Thermo-humidity cycle

In the second test, the goal was to assess the effects of thermal stress and moisture together, to have a situation closer to reality. This was carried out by fixing the welds at

both ends on a steel jig to prevent them from shifting away due to thermal expansion; the jig was placed in a CTS C-40/350 climatic chamber where the samples underwent four times the cycle shown in Figure 3.18. Potential galvanic corrosion from direct contact between aluminum and the steel jig was avoided by placing a small aluminum plate in between, necessary to keep the joint horizontal as well.

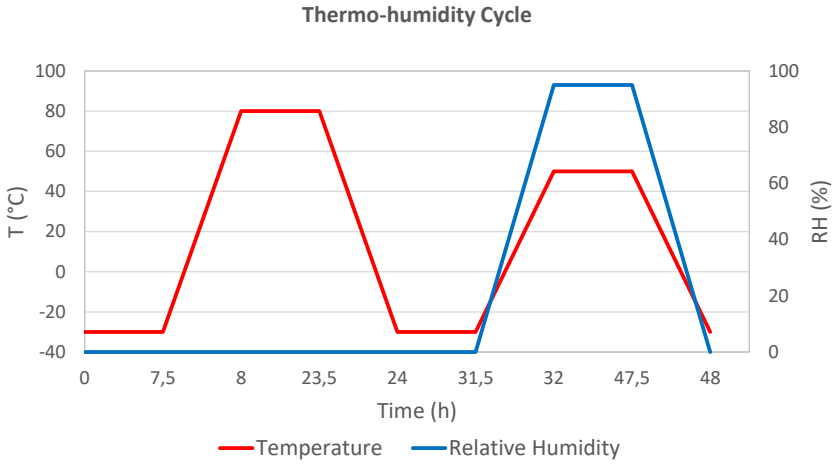

Figure 3.18: *Thermo-humidity cycle to assess thermal stresses and moisture effects*

3.3 Conclusion

In this chapter, all the different techniques and technologies employed in this research were presented, focusing on the materials and on the methods used to create, test and analyze the joint. Special attention was given to the description of all the surface pre-treatments planned and carried out on the aluminum substrates.

Chapter 4

Results: Welding Process

In the first part of the research, the focus was on the welding process itself. The most important goal was to obtain a successful reference joint without any special treatments of the substrates, differently from Bolt [5] whose specimens had to be coated before welding, and to understand the adhesion mechanisms.

4.1 Weld Configuration Evaluation

At the beginning of the research, it was observed that welding was successful only when aluminum substrate was on top, in contact with the sonotrode; when aluminum was the bottom substrate and the CFRP was in contact with the sonotrode, no bonding between the two adherends was obtained. Therefore, as mentioned in Section 3.2.1, both configurations were investigated to understand the reason for this behavior. In the following chapters, when referring to a joint configuration (i.e. material_1/material_2) the first term is the top substrate and the second term is the bottom substrate. It is important to mention that using aluminum as top adherend, there was a metal-to-metal contact with the sonotrode: this led to a fretting damage on the aluminum surface. To prevent it, a thin Kapton film (0.05mm) was placed between the aluminum and the sonotrode, with the result of an unaffected surface after welding.

4.1.1 Process Monitoring

In order to monitor the welding process, power-displacement curves were used. The curves obatined using the final parameters (500N, 34.5 µm) for the combination of Al/CFRP_1 and Al/CFRP_2 can be seen in Figures 4.1 and 4.2. One of the most significant observations was that stages very similar to thermoplastic-to-thermoplastic welding could be recognized (Fig. 2.5) [9, 11]. For both combinations 5 welds were performed: the first two welds were welded at 100% displacement, the rest around the end of stage 4, so 55% displacement for Al/CFRP_1 and 37% displacement for Al/CFRP_2.

The second observation was that for each configuration all the curves almost overlap for the most part, showing very good reproducibility of the process. For the 100% displacement, similar welding times (corresponding to the vibration phase) can be observed between Al/CFRP_1 and Al/CFRP_2, between 900 and 1100ms;

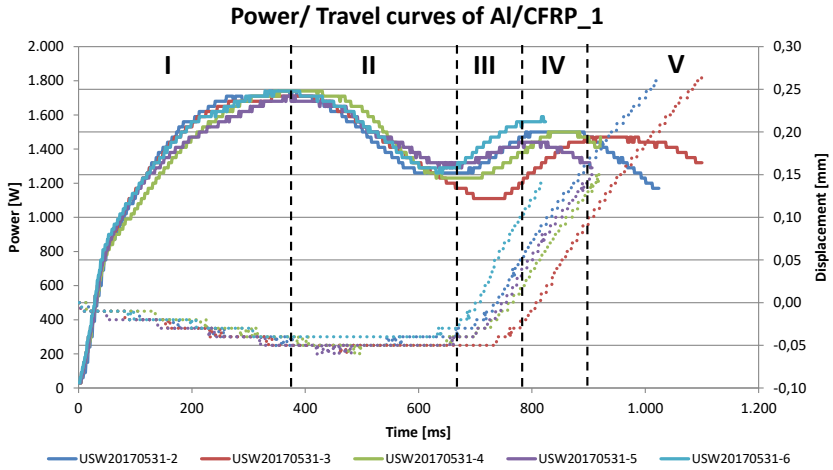

Figure 4.1: *Power-displacement curves of 5 welds in the combination Al/CFRP_1. Roman numbers indicate the different welding stages mentioned in Chapter 2 and in literature. Welding force=500N, welding amplitude=34.5 µm. The first two welds were performed at 100% displacement, the rest at 55% displacement*

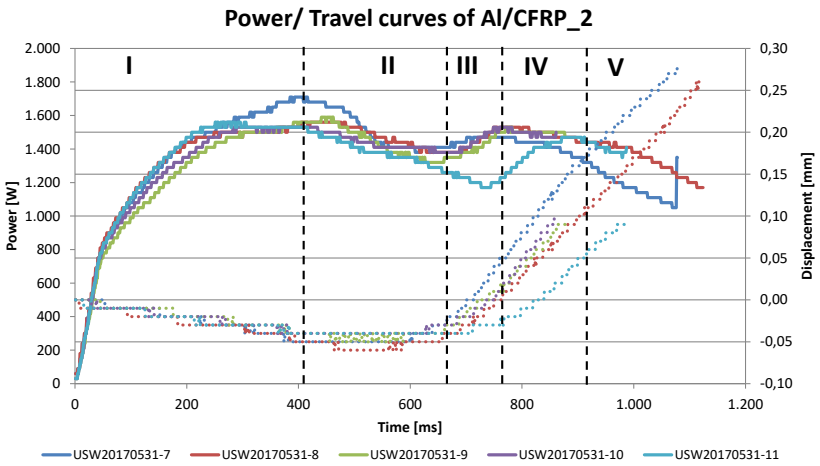

Figure 4.2: *Power-displacement curves of 5 welds in the combination Al/CFRP_2. Roman numbers indicate the different welding stages mentioned in Chapter 2 and in literature. Welding force=500N, welding amplitude=34.5 µm. The first two welds were performed at 100% displacement, the rest at 37% displacement*

Power-displacement curves for the configuration with the aluminum on the bottom, CFRP_1/Al, can be seen in Figure 4.3 (top). As mentioned earlier, welding was not successful at first in this configuration: however, placing an insulating Kapton film (thickness=0.10mm) between the aluminum and the jig made welding successful. Since the aluminum substrate is in full contact with a large steel jig, it was believed that a large

amount of heat was dissipated from the interface to the jig due to high heat conductivity of aluminum; if that was the case, it was thought that using the Kapton could avoid this phenomenon. The power-displacement curves of successful CFRP_1 /Al welds can be seen in Figure 4.3 (bottom). By overlapping the curves in these two different conditions (Fig. 4.4) it was observed that successful welds with Kapton show shorter welding times (1200 vs 1600ms), which was consistent with the hypothesis of reduced dissipated heat.

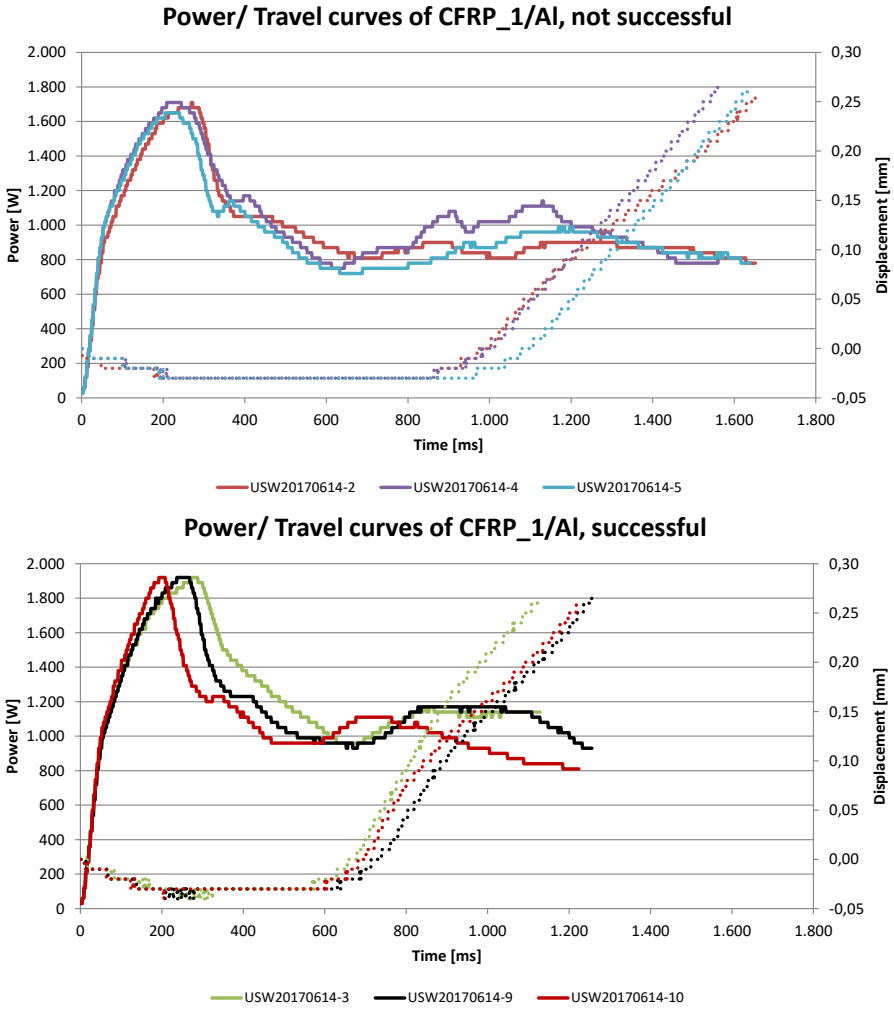

Figure 4.3: *Power-displacement curves of CFRP_1 /Al when bonding was not achieved (top) and when it was achieved using a Kapton film between metal and jig (bottom). Welding force=500N, welding amplitude=*34.5 µm*, 100% displacement*

4.1.2 Temperature Measurements

To further confirm the hypothesis of different temperatures at the interface, some temperature measurements were carried out, as explained in Section 3.2. Three measurements for successful welds (Al/CFRP_1 configuration or CFRP_1/Al with Kapton between aluminum and steel jig) and three measurements for unsuccessful welds (CFRP_1/Al with full contact between aluminum and steel jig) were peroformed. Time-temperature examples

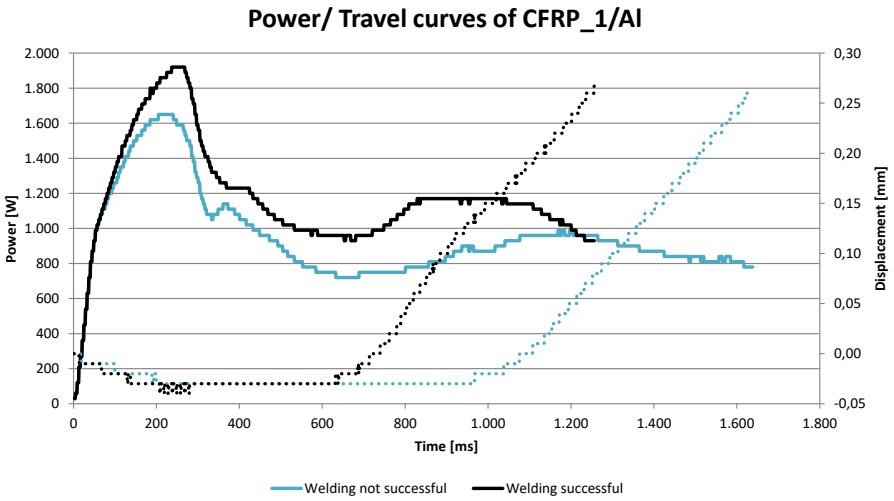

Figure 4.4: *Overlapped curves of CFRP_1 /Al when bonding was and was not achieved. Differences especially in time can be observed*

of a successful and an unsuccessful case are shown in Figure 4.5; all the measurements can be seen in Appendix D. When welding was successful, the temperatures at the interface were quite higher (average of 3 samples=492°C, ±26°C) than for the cases where welding was not successful (average of 2 samples=347°C, ±37°C). Thus, from these results it was confirmed that the Kapton film influences to a certain extent the temperature at the interface, allowing bonding between substrates to occur also when aluminum is the bottom adherend. However, it is necessary to mention that thermocouples are free to move in three dimensions inside the molten energy director, so this could lead to inaccurate measurement of the temperature at the interface. This was the case shown in Figure D.4 (bottom) where the temperature was much higher than the other measurements even if welding was unsuccessful: after joint fracture it was observed that the thermocouple actually moved completely to the edge of the overlap, which is known to experience higher temperatures [13]. Since in all other cases the thermocouple was found in the center of the overlap, the measurement was not included with the others because it was not representative.

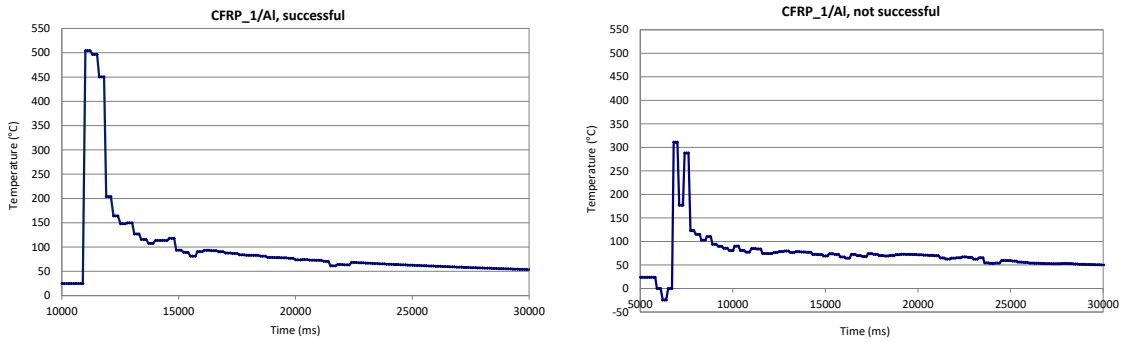

Figure 4.5: *Example of time-temperatures profile when welding was successful (left) and unsuccessful (right)*

With a second set of measurements, done by placing a thermocouple in the metal sample (see Sec. 4.1.2), the hypothesis of different temperatures was only partially confirmed. As can be seen in Figure 4.6, it is very clear that temperature in the aluminum is higher ($\approx$ 400°C vs $\approx$ 270°C) when the metal is the top substrate, but it seems that using the Kapton film when the aluminum is on the bottom does not affect significantly the temperature in the metal ($\approx$ 280°C). This difference could come from the fact that the thermocouple was not properly insulated inside the metal hole; thus, inconsistent or inaccurate measurements could be obtained.

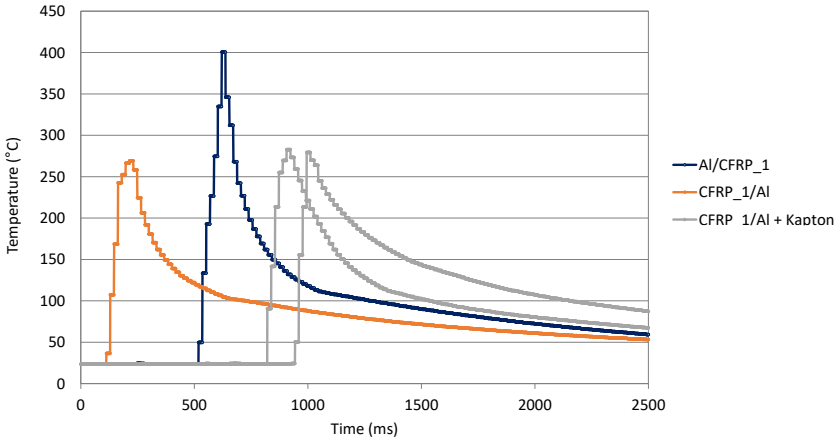

Figure 4.6: *Time-temperature curves using Aluminum and CFRP_1 with the thermocouple in the middle of the metal substrate. Welding was successful when Al was on top and when Kapton film was used with Al on the bottom.*

A difference in absolute temperatures between the first set (thermocouple embedded in the ED) and the second set (thermocouple is the metal) of measurement was also observed: this could be explained by an expected temperature gradient between the interface and the adherend, as acknowledged in literature [52, 53].

4.2 Joint Performance and Analysis

4.2.1 Lap Shear Strength

In order to quantify the joint quality, the lap shear strength (LSS) test is very common and it allows the comparison of different joint configurations. LSS results in standard conditions (23°C) are shown in Figure 4.7 and values are reported in Table 4.1; joints were created using the same parameters previously mentioned: 500N, 34.5 µm and 100% displacement. Even if 100% displacement might not have been the optimum setting for maximum strength, it was chosen as a standard criterion for an easier comparison and to reduce the number of tests. At least 3 samples per configuration were tested.

A lower strength was obtained with both Al/CFRP_2 and CFRP_2/Al compared to Al/CFRP_1 and CFRP_1/Al respectively: this could be explained by higher peak stresses at the edges of the overlap due to a higher difference in stiffness between aluminum and CFRP_2 compared to aluminum and CFRP_1 [54].

Both with CFRP_1 and CFRP_2, slightly higher LSS is obtained when aluminum is the bottom substrate and the Kapton film is used. To understand this difference, fracture surfaces were observed (Sec. 4.2.2).

Besides, with CFRP_1, a higher scattering was observed when aluminum was the top substrate; however, no significant difference was found among the power-displacement curves, so the scattering could be due to inaccurate surface preparation of the substrates.

Table 4.1: *Lap shear strength (LSS) for different joint configurations*

Configuration	**LSS** [MPa] (C.o.V)
Al/CFRP_1	6.61 (12.53%)
CFRP_1/Al+Kapton	7.16 (4.95%)
Al/CFRP_2	5.85 (3.93%)
CFRP_2/Al+Kapton	6.94 (5.31%)

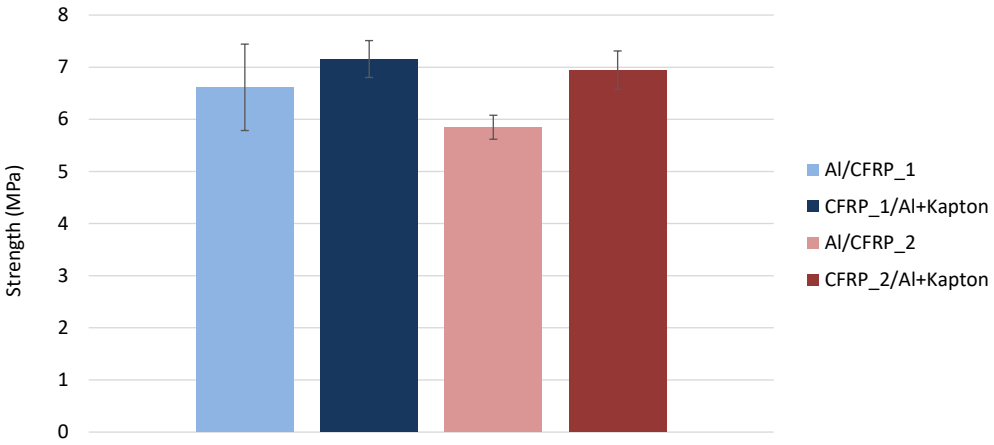

Figure 4.7: *Comparison of LSS for different joint and material configurations*

Adhesive joints were prepared and tested as explained in Section 3.2.2, to evaluate how ultrasonic plastic welding compares with other joining technologies. Strengths of 14.70 MPa (C.o.V=2.96%) and 10.53 MPa (C.o.V=7.15%) for Aluminum and CFRP_1 and Aluminum and CFRP_2 were obtained respectively, showing that without specific surface pre-treatments, ultrasonic plastic welding was inferior to adhesive bonding.

4.2.2 Cross Sections and Fracture Surfaces

After being tested, joints were analyzed observing the fracture surfaces. To help the reader understanding the following discussion, a schematic of the joint with the nomenclature used can be seen in Figure 4.8.

First of all, it was very clear that there were two different types of failures occurring due to different bonding along the overlap (Fig. 4.10). The area close to the metal edge

presents a first-ply failure, where fibers are pulled out from the composite and remain attached to the metal surface; moving towards the CFRP edge, failure becomes adhesive. This suggests that stronger bonding between the CFRP and the aluminum takes place in the former mentioned area.

The hypothesis is that the metal edge experiences higher temperatures due to edge effect [13], while on the CFRP edge heat is easily transferred to the whole aluminum sample due to high thermal conductivity. The higher temperatures on the metal edge lead to a lower viscosity of the molten polymer, which is able to create stronger mechanical interlocking on a micro-level and complete contact between the two substrates.

To further confirm this, cross sections parallel to the overlap (Fig. 4.9) were examined.

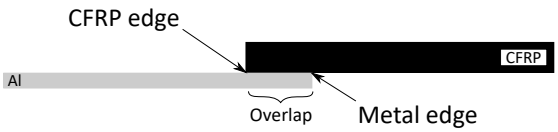

Figure 4.8: *Schematic of the joint with the nomenclature used in this report*

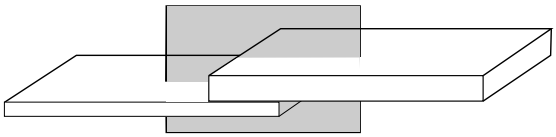

Figure 4.9: *Schematic of the position in the weld where cross sections are taken*

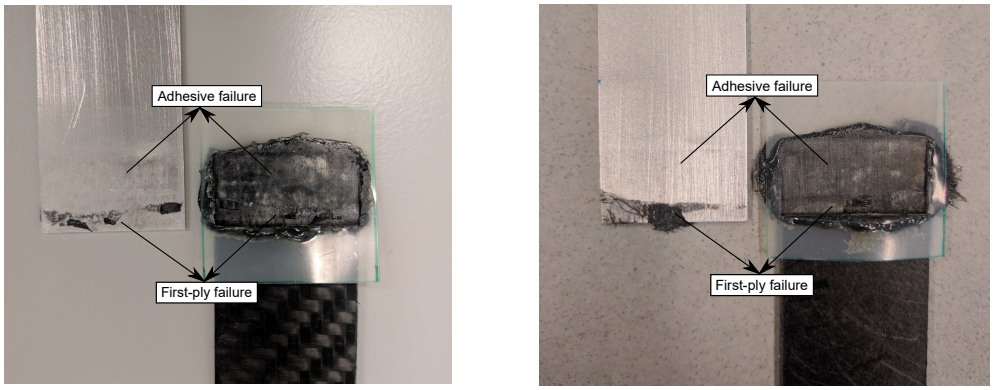

Figure 4.10: *Fracture surfaces of CFRP_1/Al (left) and CFRP_2/Al (right). In both cases different types of fractures are visible along the overlap*

In Figure 4.11 the area close to the metal edge is visible for the Al/CFRP_1 configuration: all aluminum micro-cavities are completely filled with resin. In the region close to the CFRP edge (Fig. 4.12), it is quite clear that complete filling was not obtained. The same conclusions could be drawn with CFRP_1/Al configuration (Fig. 4.13, 4.14).

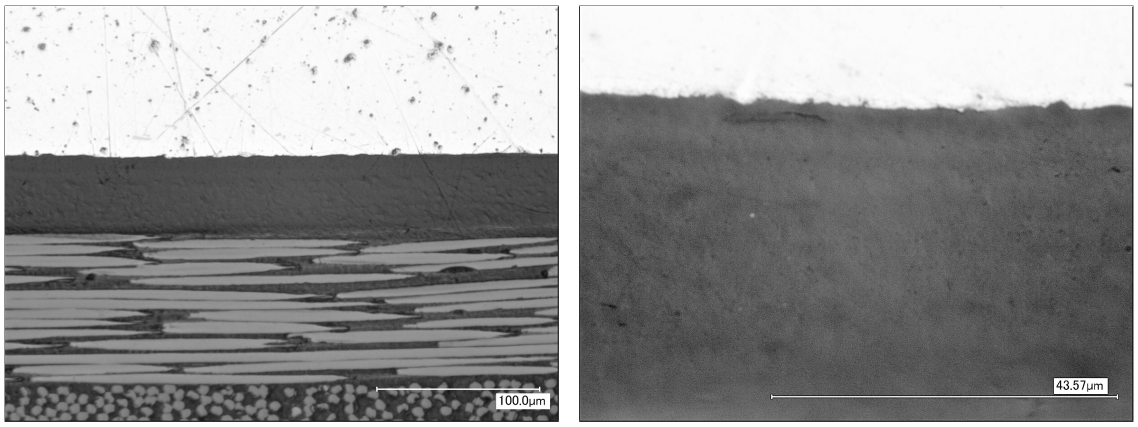

Figure 4.11: *Magnifications of Al/CFRP_1 interface close to the metal edge. Complete filling of metal roughness is visible. Parameters: 500N,* 34.5 µm*, 100% displacement*

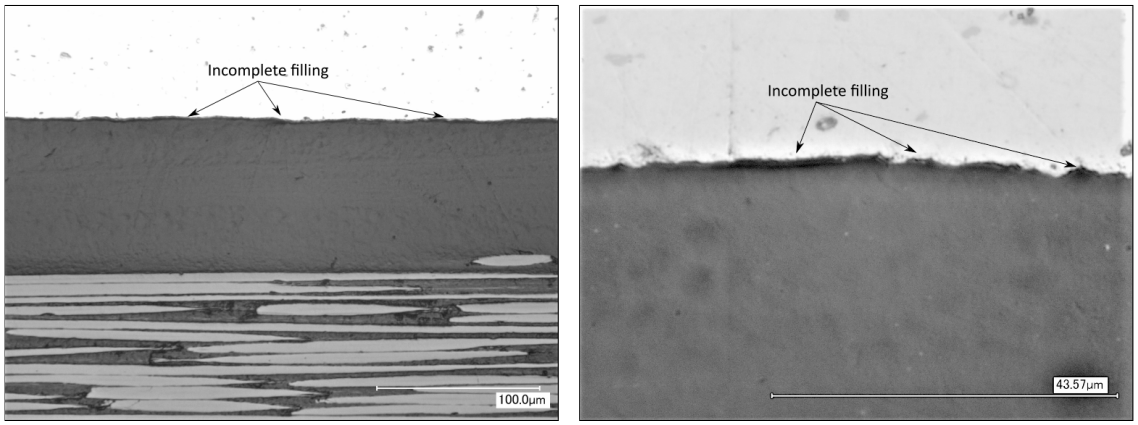

Figure 4.12: *Magnifications of Al/CFRP_1 interface close to the CFRP edge. Incomplete filling of metal roughness is visible. Parameters: 500N,* 34.5 µm*, 100% displacement*

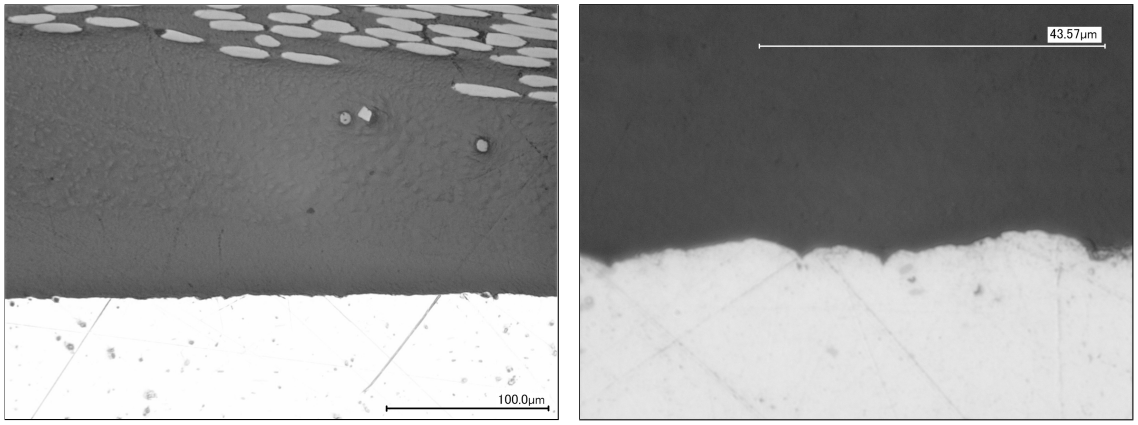

Figure 4.13: *Magnifications of CFRP_1/Al interface close to the metal edge. Complete filling of metal roughness is visible Parameters: 500N,* 34.5 µm*, 100% displacement*

Similar results were obtained by Ageorges and Ye [12] for resistance welding between Al 7075-T6 and CF/PEI and by Mitschang et al. [15] for induction welding between AlMg3

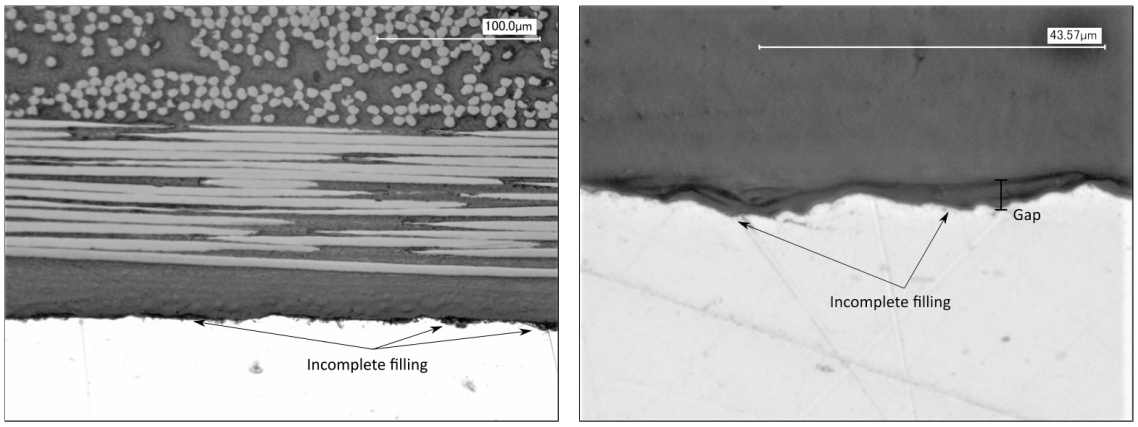

Figure 4.14: *Magnifications of CFRP_1/Al interface close to the CFRP edge. Incomplete filling of metal roughness is visible. Parameters: 500N,* 34.5 µm*, 100% displacement*

and CF/PA66. For future developments, higher strengths can be expected if the whole overlap could behave like the first area.

A second observation was made regarding the difference between the configuration with aluminum as top or bottom substrate: looking at Figure 4.15, it is possible to see that when aluminum was the bottom substrate (with Kapton film), more fibers were usually found on the metal surface. This is consistent with the higher strengths obtained in this configuration (see Fig. 4.7), and it is possibly due to the higher insulating effect of the thicker Kapton film. For this reason, in the rest of the study aluminum was always used as the bottom substrate.

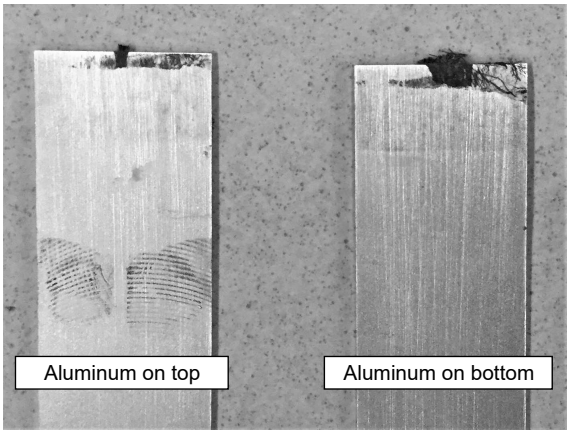

Figure 4.15: *Difference between top and bottom configuration with aluminum and CFRP_2. First-ply faliure area is larger when aluminum is the bottom substrate*

4.3 Conclusion

In the first part of the research, the focus was on the welding process itself and on the adhesion behavior. Welding aluminum to CFRP_1 and CFRP_2 proved to be successful,

both with the aluminum as top substrate and the aluminum as bottom substrate: welding in the latter case was achieved by placing an insulating Kapton film between the metal adherend and the metal welding jig, to avoid excessive heat dissipation from the interface.

When compared to thermoplastic-to-thermoplastic ultrasonic plastic welding, similar results were obtained in terms of process monitoring and reproducibility: also in the case of metal-to-thermoplastic welding the process is reliable and consistent when controlled by sonotrode displacement. However, strengths obtained were quite lower compared to adhesive joints, the reference joining technology.

Finally, it was observed that in the weld the area close to the metal edge experiences stronger adhesion resulting in first-ply failure, while the rest of the overlap presents adhesive failure; it is believed that the main cause was a non-uniform temperature distribution along the overlap.

Chapter 5

Results: Surface Treatments

As mentioned in Chapter 2, surface pre-treatments of the metal substrate represent a possible way of obtaining stronger and more durable joints. In this chapter, the influence of all treatments described in Section 3.2.6 on the adhesion mechanisms and on the joint performance is discussed. Unfortunately, AMALPHA treatment was eventually not evaluated since it took too long to arrange this treatment

5.1 Surface Analysis

Since the main bonding mechanisms occurring during welding (mechanical interlocking, adsorption) strongly depend on the metal surface properties, it is important to analyze how the pre-treatments alter the aluminum surface. Different techniques were employed to characterize surface morphology, chemical composition, topography and wettability.

5.1.1 Surface Morphology and Chemical Composition

Scanning electron microscopy (SEM) along with energy dispersive X-ray spectrometry (EDS) were used to examine the morphology and the chemical composition of the aluminum surface after selected treatments.

SEM

The surface of a sample without treatments (only degreased) can be seen in Figure 5.1: the effects of the rolling process are visible, forming some kind of waviness on the surface; besides, many impurities were still present on the surface.

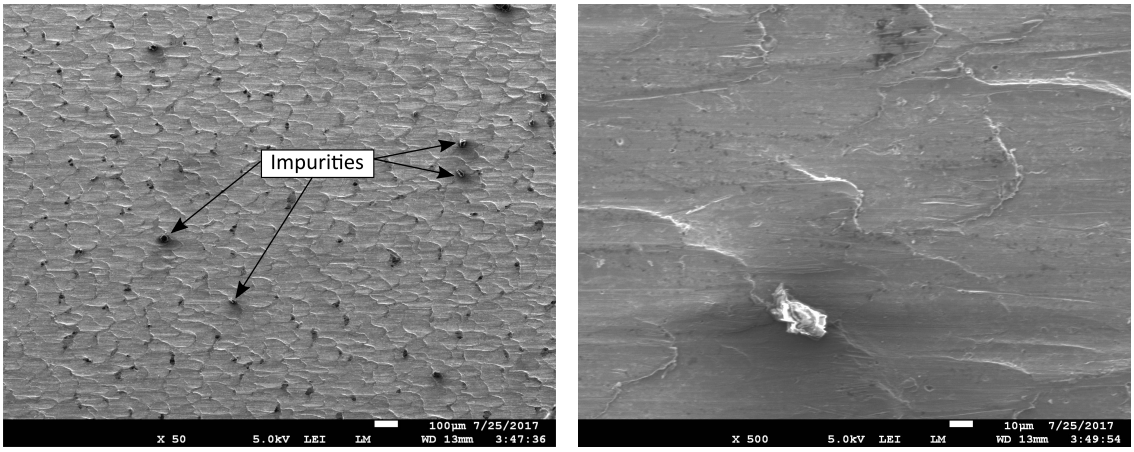

Figure 5.1: *Aluminum surface without pre-treatments. Many impurities can be observed*

Sandblasting produced a much rougher surface (Fig 5.2) with different irregular shapes due to the alumina particles.

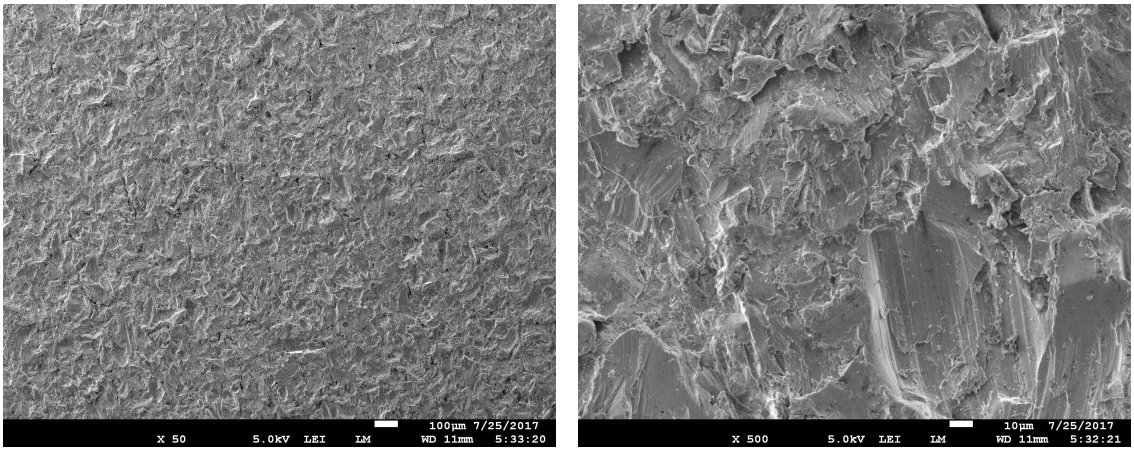

Figure 5.2: *Aluminum surface after sandblasting treatment. High roughness with irregular shapes can be observed*

Grooves created by laser treatment are clearly visible in Figure 5.3 for the Galvo Scanner mode and Polygon Mode: it is possible to see the differences in pitch distance, groove width and groove depth.

Both plasma treatment and acid pickling showed extremely clean surfaces compared to the untreated samples (Fig. 5.4). In contrast, treating the aluminum with both alkaline and acid solutions produced a large amount of very small pits on the surface, due to the aggressive action of NaOH (Fig. 5.5).

Finally, the conversion coating formed a layer with small particles on the surface (Fig. 5.6): however, the particles do not cover the whole surface, probably due to the short immersion time of the sample in the Bonderite solution; the influence of parameters such as duration of pre-treatment, concentration of solution, temperature etc. on the formation of the conversion layer was not considered because it was beyond the scope of this research.

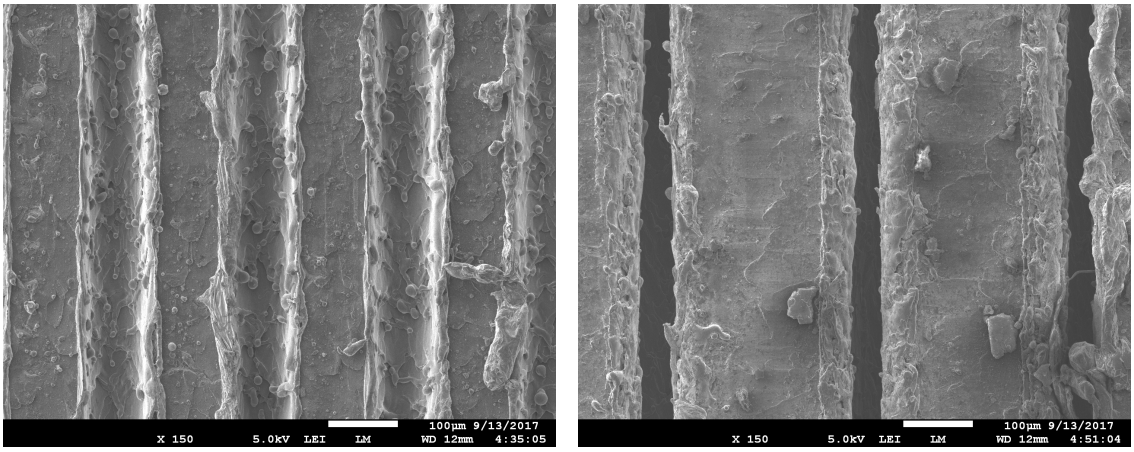

Figure 5.3: *Laser grooves created by Galvo Scanner mode (left) and Polygon mode (right)*

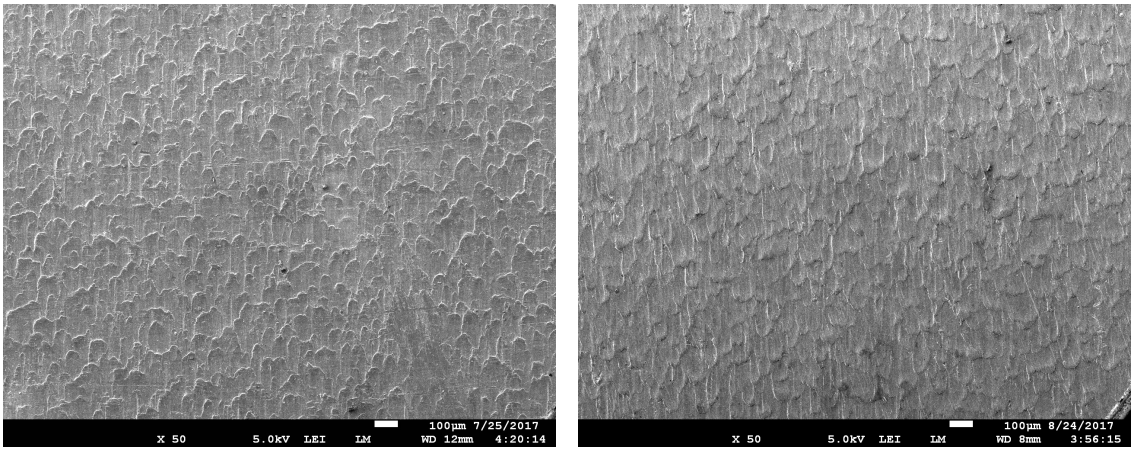

Figure 5.4: *Impurities on the aluminum surface were entirely removed by plasma treatment (left) or acid pickling (right)*

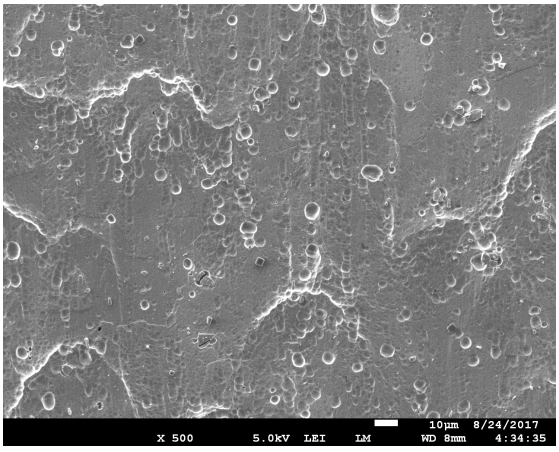

Figure 5.5: *Pits on the aluminum surface after alkaline-acid etching*

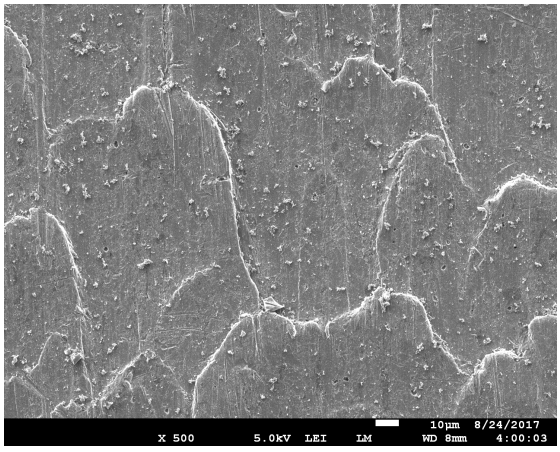

Figure 5.6: *Particles of the conversion coating layer on the aluminum surface*

EDS

The chemical composition of the metal surface is a very important parameter involved in the adsorption of the thermoplastic. Obtaining a quantitative value of the elements present on the surface can help understanding the behavior of substrates during welding and how this affects the joint performance.

Some interesting observation can be made from Table 5.1, which shows the composition of the aluminum samples after different treatments. First of all, it is relevant to remark that most treatments produced results close to the expectations (see Sec. 3.2.6): both types of etching and plasma removed a large amount of organic contaminants, indicated by the decreasing amount of carbon on the surface. After plasma treatment, even a small amount of titanium and zirconium was detected, probably from the very thin coating of the original sample (Sec. 3.1). The presence of the chromium and zirconium conversion coating was confirmed as well; the Cr and Zr values are very small probably due to the small amount of the coating, as seen in the SEM pictures (Fig. 5.6). Alkaline-acid etching shows a higher amount of aluminum, a confirmation of the removal of the outer layer from the original surface. Conversely, a lower concentration of aluminum was found in sandblasted sample, along with a higher amount of oxygen: this is consistent since Al_2O_3 was used as blasting medium, which increased the amount of oxide on the surface. Sandblasting also increased the surface area, which could adsorb more contaminants, hence the slightly higher amount of carbon found.

In samples without treatments or after plasma treatment, F was found as well in small amounts: this is likely coming from the manufacturing process of the aluminum and was not removed by the pre-treatments.

Table 5.1: *Chemical composition (wt%) of the aluminum surface after different pre-treatments, analyzed by EDS*

	No treatment	Sandblasting	Alkaline-acid Etching	Acid Pickling	Conversion Coating	Plasma
Al	75.48	65.56	82.31	76.41	70.26	76.75
O	3.12	9.66	2.08	7.78	6.54	4.66
C	20.93	23.22	14.57	14.97	21.52	16.86
Mg	0.19	0.22	0.25	0.30	0.24	0.24
Si		0.62	0.79	0.55	0.72	0.60
Ti						0.26
Zr					0.53	0.12
Cr					0.04	
Fe		0.74				
F	0.28					0.51

5.1.2 Surface Topography

EDS gives a useful insight to understand the role of the pre-treatments in terms of adhesion forces. To quantify the difference between the pre-treatments in terms of mechanical interlocking, the surface roughness (R_a and R_q) was measured through a Confocal microscope. Results are shown in Table 5.2. and an example of the surfaces topography can be seen in Figure 5.7.

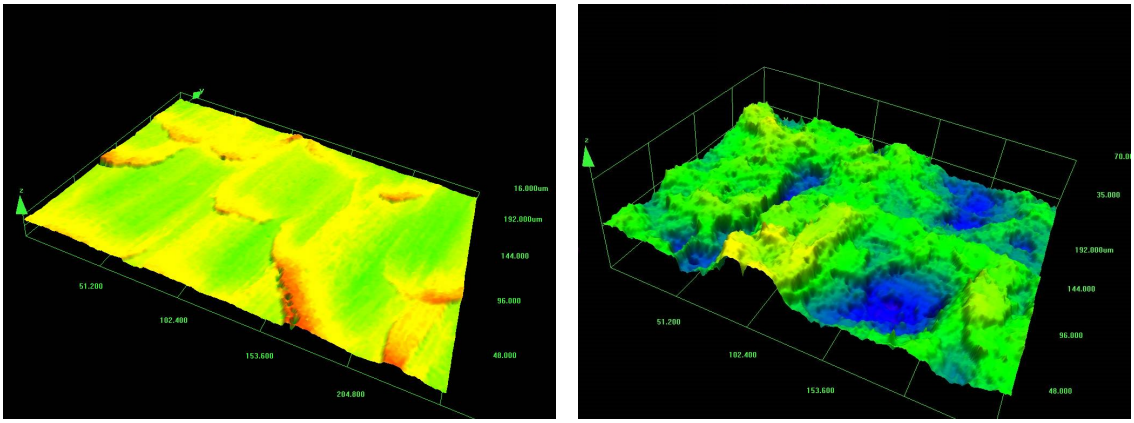

Figure 5.7: *Surface roughness measured by the Confocal microscope for an untreated sample (left) and a sandblasted sample (right)*

Table 5.2: *Surface roughness values obtained by the Confocal microscope for different pre-treatments. One sample per treatment was analyzed*

	No treatment	Sandblasting	Alkaline-acid Etching	Acid Pickling	Conversion Coating	Plasma
R_a	0.83	5.20	1.06	1.01	0.85	1.07
R_q	1.05	6.56	1.33	1.29	1.15	1.44

Chemical and physical pre-treatments did not change significantly the roughness, which increased only a little. Conversely, sandblasting created a much rougher surface, as seen also with SEM in Section 5.1.1. Higher R_a and R_q means a larger bonding area and thus a larger amount of molten CFRP in contact with the metal, effectively increasing the mechanical interlocking.

5.1.3 Surface Wettability

Another method to characterize surface properties was measuring the contact angle between a 5mL droplet of DI water and the aluminum. This gives easy and fast indications of the wettability of the surface. If the contact angle is low (good wettability), higher surface energy of the substrate is obtained, allowing better adhesion [4, 55]. Measurements were done on at least four different samples, and the results can be seen in Table 5.3.

Table 5.3: *Water contact angle measurement on the aluminum surface after different pre-treatments*

	No treatment	Sandblasting	Alkalkine-acid Etching	Acid Pickling	Conversion Coating	Plasma
θ °	85 (±5)	72 (±6)	103 (±3)	65 (±3)	33 (±8)	34 (±4)
	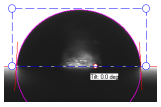	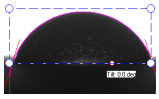	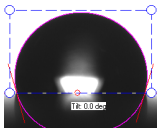	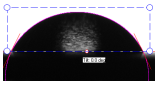		

Plasma and conversion coating showed a much smaller contact angle compared to the untreated aluminum, revealing a better wettability; this is probably because of a lower amount of contaminants, activation of the surface and the different chemical composition as seen with SEM-EDS. However with acid pickling, also used to remove contaminants, higher contact angles were found, but still better than on the untreated surface.

Sandblasting shows a lower value compared to untreated aluminum as it is well known that higher roughness enhances wettability [56, 57]; however, the high amount of carbon found by the EDS could explain why the value is only slightly lower than the untreated surface.

Finally, alkaline and acid etching increased the wetting angle, which is in contrast to what is expected from the EDS results. It might be that samples were not cleaned properly after etching and that some residual of the solutions were still present on the surface.

5.2 Lap Shear Strength and Joint Analysis

In the previous section the differences in surface modification between several aluminum pre-treatments were investigated. To quantify the improvements expected in joint performance, the lap shear strength of welds between treated aluminum and both CFRP_1 and CFRP_2 was evaluated. The welds were analyzed before and after fracture. A summary of the parameters used for each treatments can be seen in Table 5.4.

The first observation right after all tests was that the aluminum was slightly bent at the end of the overlap. This is typical in single-lap joints due to the load eccentricity, which induce peel stresses at the edges of the overlap.

Table 5.4: *Summary of welding conditions for each treatment in terms of welding force, amplitude and sonotrode displacement*

Treatment	Welding parameters
Sandblasting Conversion Coating Alkaline-acid etching Acid pickling Plasma	With ED 500N 34.5 µm 100% ED thickness
Laser	With ED 500N 26 µm 100% ED thickness
3D printing Metal hooks	With and without ED 500N 34.5 µm Pin/hook height

5.2.1 CFRP_1 and Aluminum

In Table 5.5 and Figure 5.8 the results of lap shear tests using aluminum substrates with different surface pre-treatments and CFRP_1 are shown; LSS of adhesive reference joints were measured as well.

Table 5.5: *LSS values for welded CFRP_1 and aluminum after different treatments. The increase compared to the untreated aluminum is shown as well.*

Treatment	**LSS** [MPa] (C.o.V)	% increase
Adhesive (reference)	14.70 (2.96%)	/
No treatment	7.16 (4.95%)	/
Sandblasting	9.87 (2.02%)	37.90
3D printing	7.96 (2.85%)	11.17
Metal hooks	7.69 (9.15%)	7.41
Laser (Galvo Scanner)	13.86 (2.53%)	93.62
Conversion Coating	10.65 (2.40%)	48.88
Alkaline-acid etching	7.37 (10.31%)	2.96
Acid pickling	8.81 (4.64%)	23.14
Plasma	9.05 (2.64%)	26.52

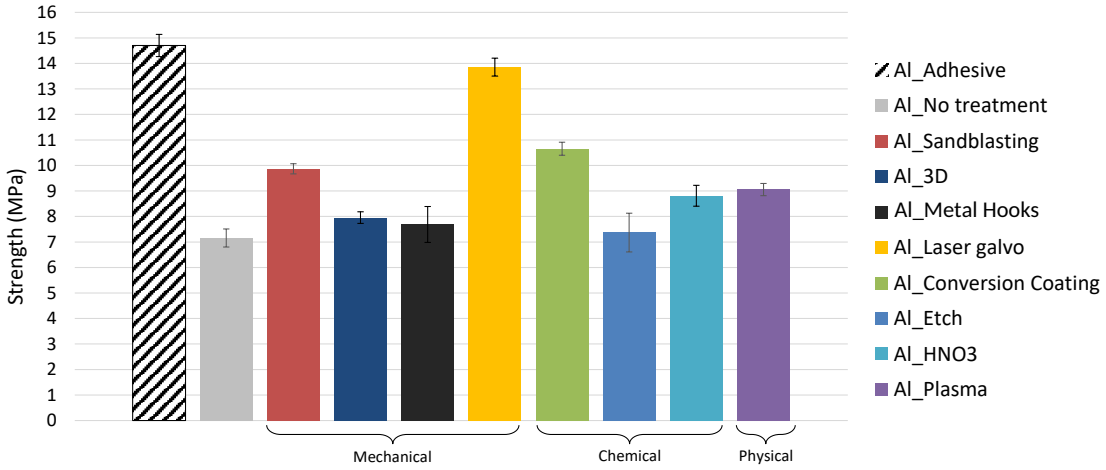

Figure 5.8: *Lap shear strength of joints with CFRP_1 and aluminum after different treatments. In the legend, Al_etch refers to the alkaline-acid etching and Al_HNO3 refers to the acid pickling*

It is possible to observe that among mechanical treatments, sandblasting and laser treatment produced the highest results, while conversion coating was the best one among the chemical treatments.

Unfortunately, welding aluminum treated by laser in Polygon mode was unsuccessful. The grooves were too deep and weakened severely the base material, which broke due to the ultrasonic vibrations. For laser treatment with Galvo Scanner, amplitude was reduced to the minimum (26 µm) to avoid potential damage: the treatment almost doubled the initial strength, with values comparable to the adhesive reference.

However, it is necessary to say that adhesive reference joints had spew fillets and thicker bondlines, which are known to influence the lap shear strength [58–61]. Conversely, weld bondlines varied from a few microns up to 100 µm depending on the position of fiber bundles and resin-rich areas of the thermoplastic.

The mechanical treatments with through-thickness reinforcements, 3D printing and Metal Hooks, did not exhibit the desired results, with only a slight strength increase; welding both with and without ED was tested and no significant difference in strength was found. Acid pickling and plasma, which simply produced a very clean surface, shows similar strength values; conversely, alkaline-acid etching did not have any significant effect, probably due to the very high contact angle which did not allow a good wetting of the surface.

To further understand the effects of the pre-treatments on the joint, cross sections and fracture surfaces were analyzed.

Cross Sections

On the basis of the results obtained in Section 5.1, the most interesting cases for cross section analysis were the mechanical treatments, since higher interlocking with the molten CFRP was expected. All the rest of the cross sections can be seen in Appendix E.

In Figures 5.9 and 5.10 the interface with sandblasted aluminum and laser structured aluminum respectively is visible. High interlocking with the thermoplastic resin is very clear, especially in the case of laser treatment.

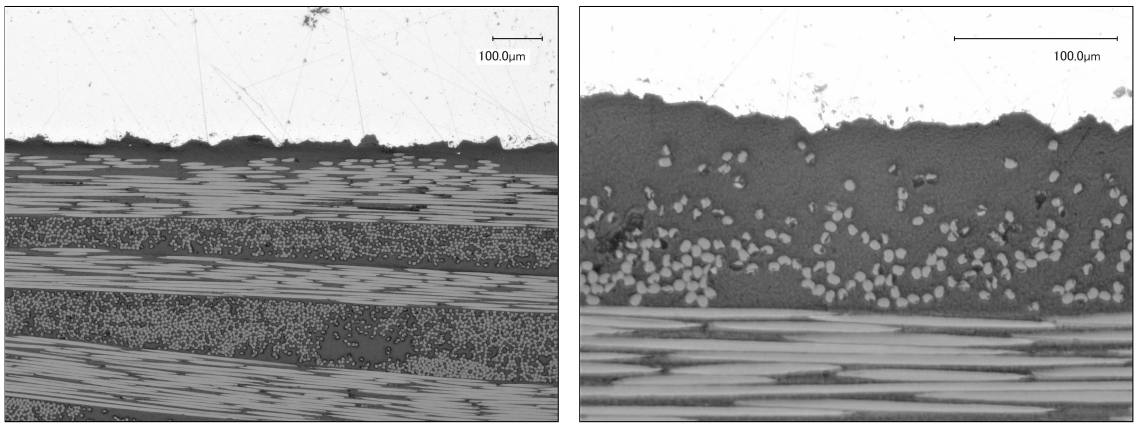

Figure 5.9: *Cross sections of a joint between CFRP_1 and sandblasted aluminum, from the center of the overlap. The aluminum surface is clearly affected by sandblasting, allowing better interlocking with the molten thermoplastic.*

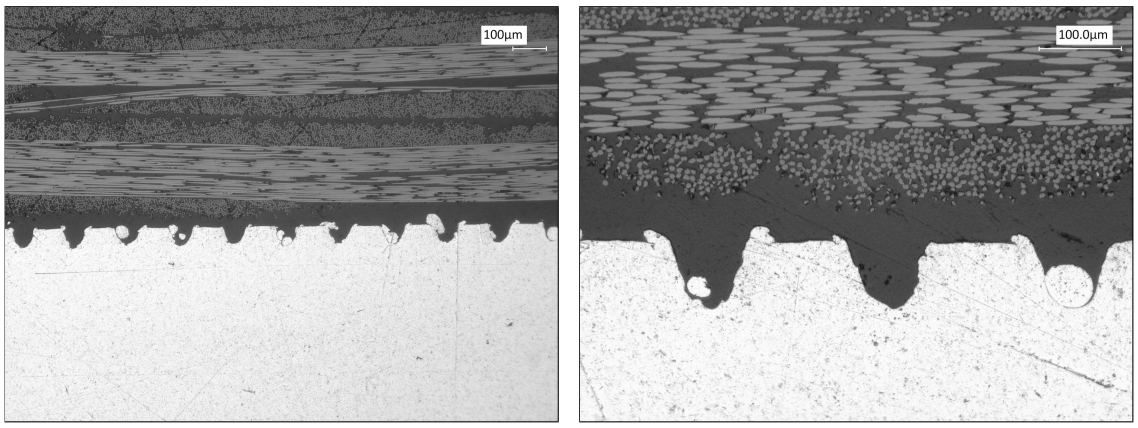

Figure 5.10: *Cross sections of a joint between CFRP_1 and laser structured aluminum, from the center of the overlap. The grooves created by the laser are visible, completely filled by the molten thermoplastic.*

It is also interesting to take a look at the cross sections with the Metal Hooks treated aluminum (Fig. 5.11). Many hooks created on the surface were highly deformed or damaged (cracks) during the welding process, preventing them from creating an effective reinforcement.

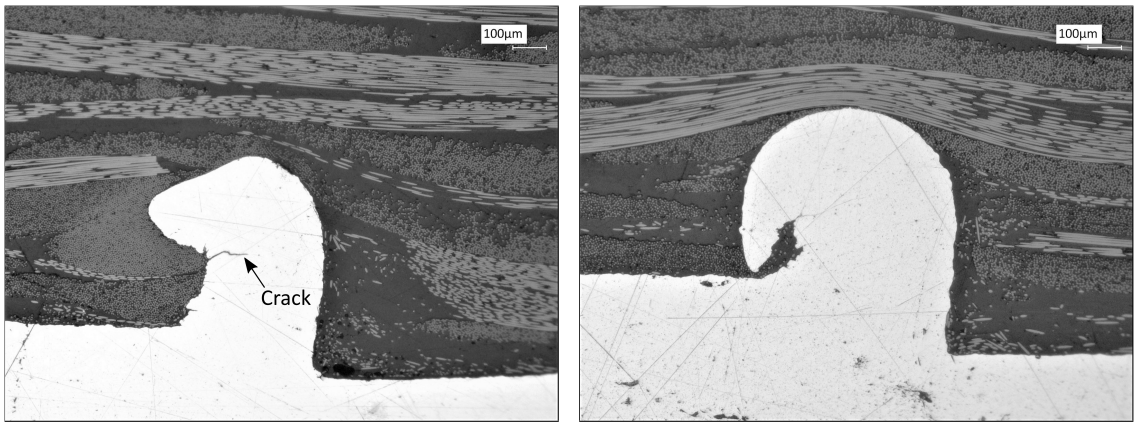

Figure 5.11: *Cross sections of a joint between CFRP_1 and Metal Hooks aluminum. Cracks and deformation of the hooks can be observed.*

Eventually, looking at 3D printed pins in the joint (Fig. 5.12) it was first found that the precision of the pins was fairly poor; besides, cracks were visible at the base of several pins.

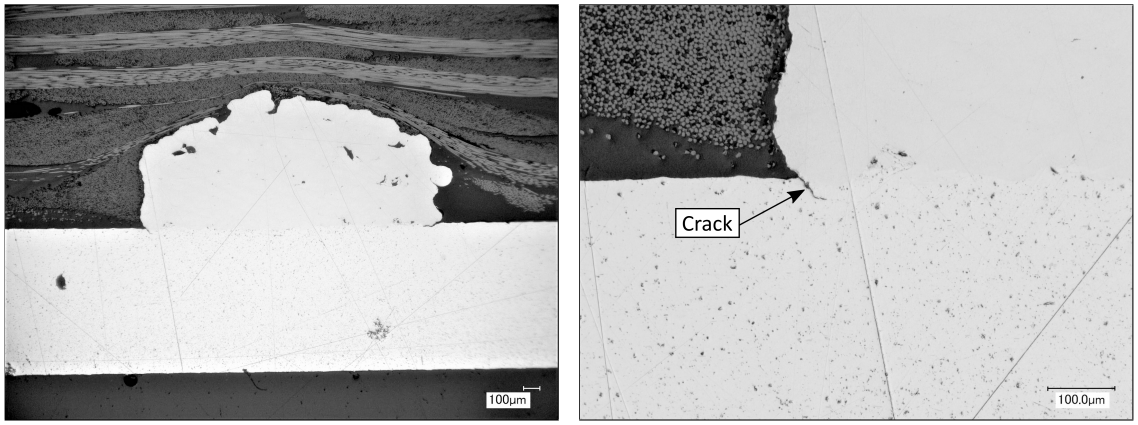

Figure 5.12: *Cross sections of a joint between CFRP_1 and aluminum with 3D printed pins.*

Fracture Surfaces

In order to gain more information on failure mechanisms using pre-treated aluminum, fracture surfaces were observed visually and by means of SEM.

Starting from the best performing treatment (laser), Figures 5.13 and 5.14 show details of both aluminum and thermoplastic substrates after failure.

On the metal part, it was evident that part of the overlap was still covered by resin filling the grooves, with some fiber bundles pulled apart from the CFRP; on the counter areas of the composite, high shear deformation experienced by the resin could be observed, which led to higher shear strengths.

A confirmation of the high stresses in the joint was given by the presence of quite large cracks which grew at the notch of the laser grooves in the aluminum; the cracks initiated either from the ultrasounds during the welding process or simply by carrying the load during lap shear tests, as the notch acts as stress concentration.

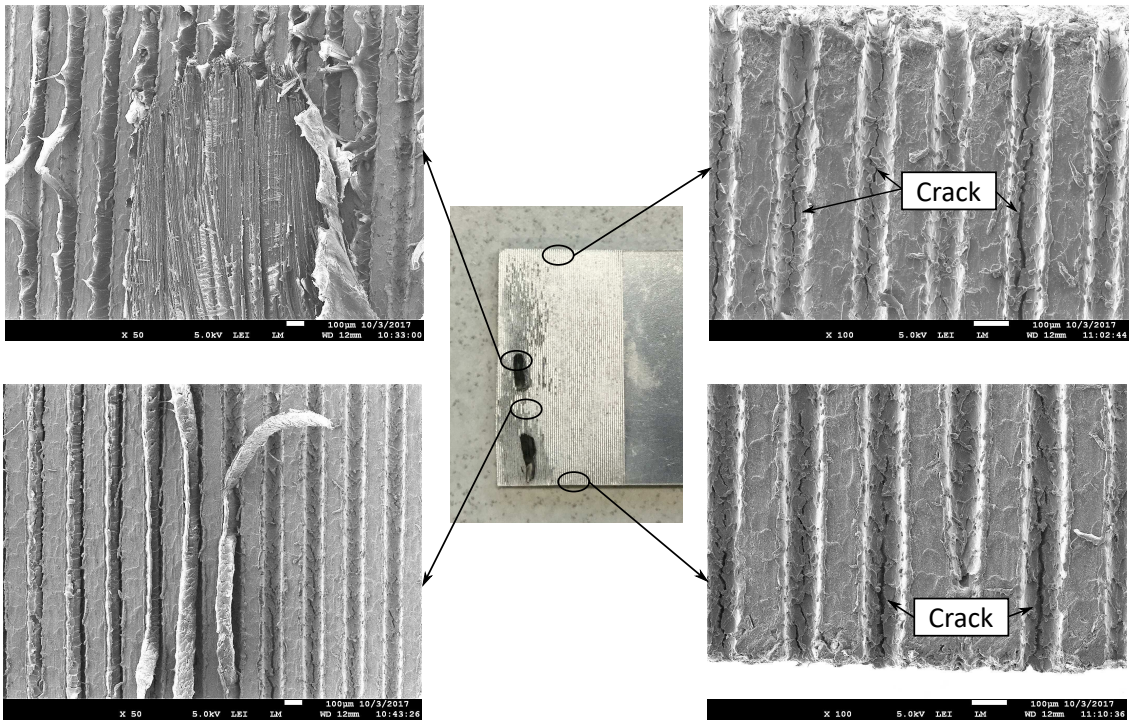

Figure 5.13: *Fracture surface of the laser treated aluminum substrate, with details analyzed by SEM.*

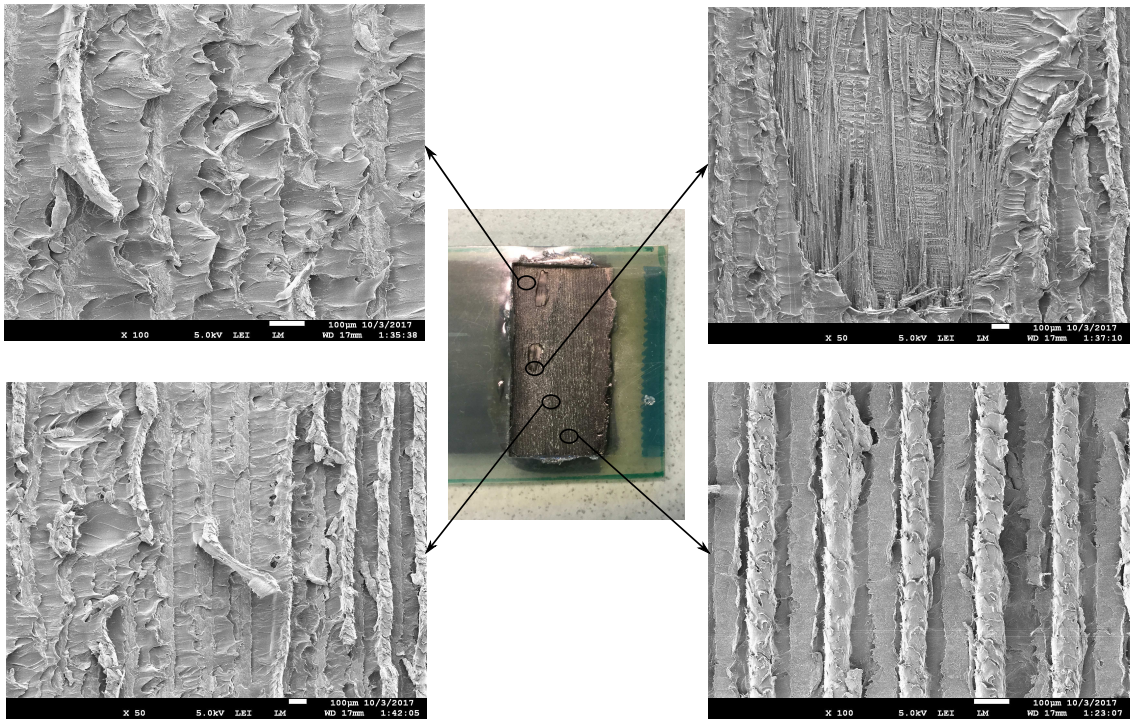

Figure 5.14: *Fracture surface of the CFRP_1 substrates after welding with laser treated aluminum; details were analyzed by SEM.*

For other treatments like sandblasting, conversion coating and plasma (Fig. 5.15), it was possible to see that the area failing by first-ply failure increased compared to the untreated aluminum joints (Fig 4.10), evidence that stronger adhesion between the two materials occurred.

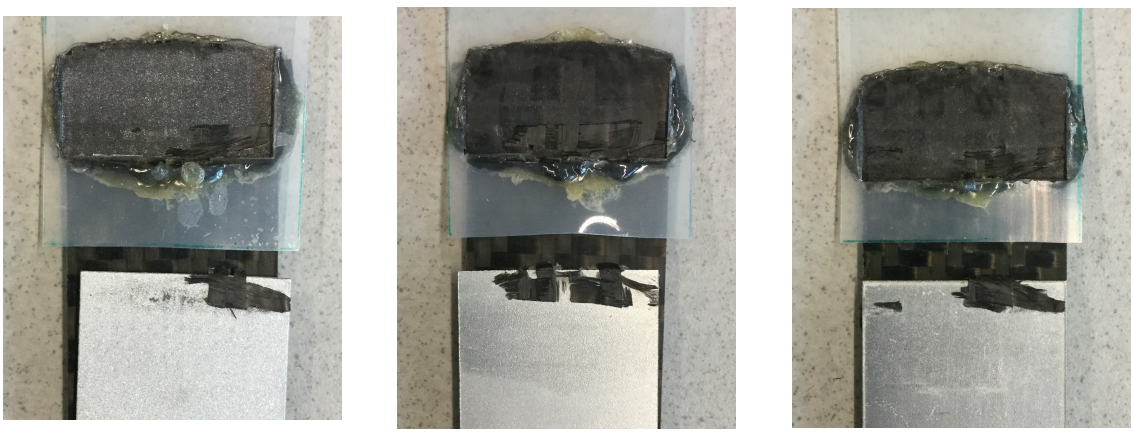

Figure 5.15: *Fracture surfaces of joints between CFRP_1 and aluminum treated with sandblasting (left), conversion coating (center) and plasma (right). Larger area covered by fibers is present on the aluminum overlap compared to untreated samples*

Among through-thickness reinforcements, CFRP_1 substrate of a weld with Metal Hooks aluminum is shown after failure in Figure 5.16 (left); no ED was used in this case. Many

delaminated hooks could still be found inside the thermoplastic, indicating that failure occurred mostly in the hooks due to defects previously observed.

Finally, in Figure 5.17, both adherends with 3D printed aluminum after failure are shown. For the CFRP substrate, SEM was used to investigate if there was a difference in failure mode between the several rows of pins. This is shown in Figure 5.18, where a hole created by a pin from the top row (left) is compared to a one from the bottom row (right).

It is possible to see that bottom rows experienced higher shear while top rows experienced a significant amount of peel as well, indicated by fiber tearing. This was consistent with the stress distribution theory for single-lap joints between dissimilar materials [62–65]: according to it, higher peak stresses are found on the edges of the overlap due to bending moments and due to stiffness imbalance.

In the aluminum sample, some fibers could be observed on the edges of a few pins, confirming that some interlocking occurred. However, from these results it was not possible to fully understand why the pins produced only a small increase in strength.

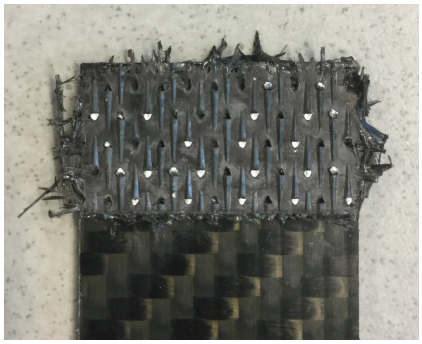

Figure 5.16: *Fracture surface of thermoplastic previously welded to Metal Hooks aluminum.*

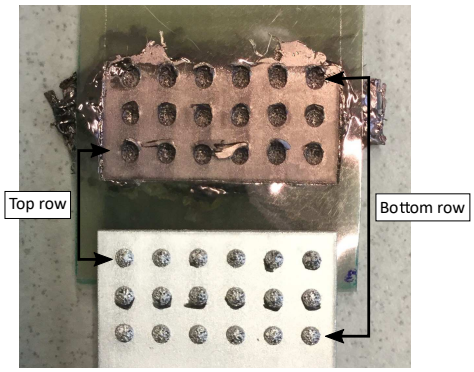

Figure 5.17: *Fracture surfaces of both aluminum with 3D printed pins and thermoplastic.*

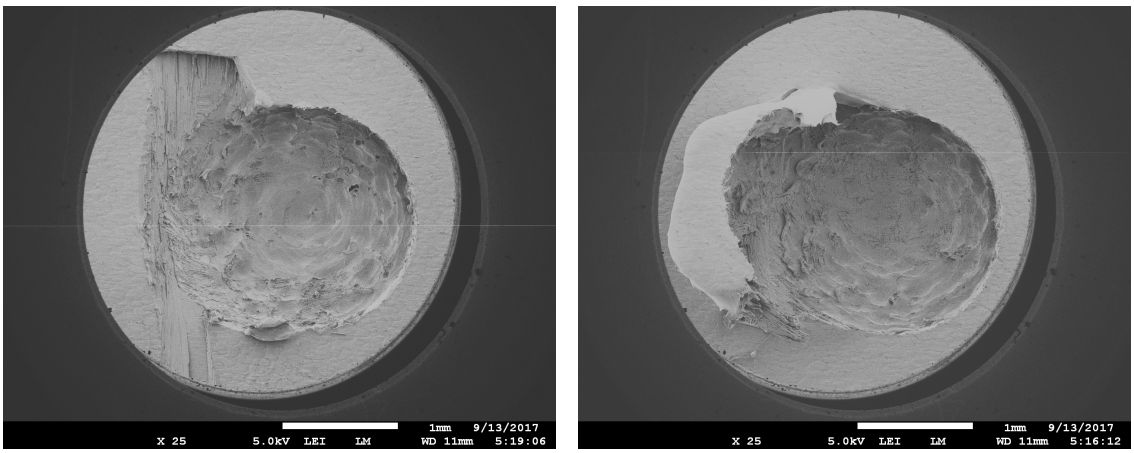

Figure 5.18: *Details of holes created in the thermoplastic by aluminum 3D printed pins after failure. Top rows (left) show some fiber bundle teared away indicating peel stresses; bottom rows (right) show much higher shear deformation.*

5.2.2 CFRP_2 and Aluminum

Unfortunately it was not possible to test the same amount of pre-treatments for the combination of aluminum and CFRP_2. Therefore, the focus was on checking if the trend was similar for some selected pre-treatments. The results can be seen in Table 5.6 and Figure 5.19.

Table 5.6: *LSS values for welded CFRP_2 and aluminum after different treatments. The increase compared to the untreated aluminum is shown as well.*

Treatment	**LSS** [MPa] (C.o.V)	**% increase**
Adhesive (reference)	10.53 (7.15%)	/
No treatment	6.94 (2.57%)	/
Sandblasting	8.44 (4.35%)	21.56
3D printing	11.64 (0.65%)	67.65
Metal Hooks	11.19 (2.48%)	61.11
Conversion Coating	8.72 (6.21%)	25.55
Plasma	7.11 (15.36%)	2.40

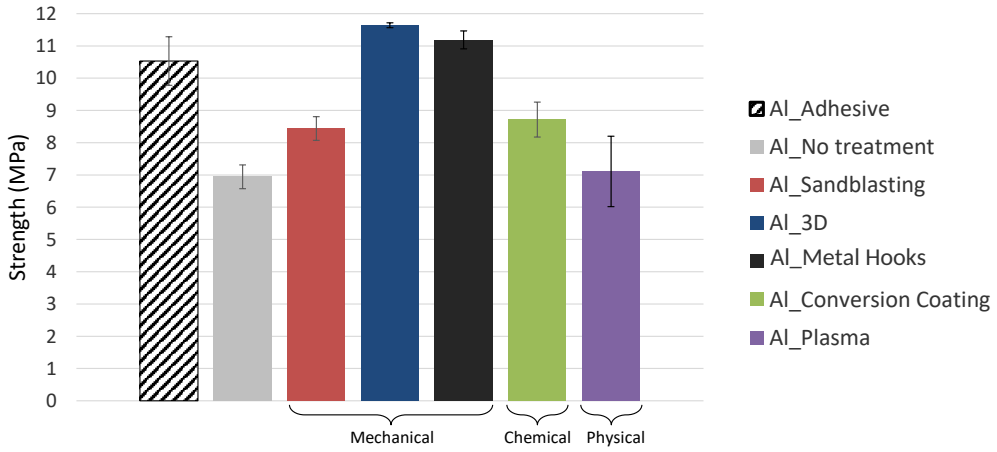

Figure 5.19: *Lap shear strength of joints with CFRP_2 and aluminum after different treatments*

For sandblasting and conversion coating a significant increase in strength could be observed again. However, plasma treatment showed a smaller improvement compared to the combination with CFRP_1 and a higher scattering: this could come from an incorrect application of the pre-treatment, which did not produce the desired effect, or a higher amount of contamination which could not be fully removed.

Instead, the most interesting results came from the welds with through-thickness reinforcements (3D pins and Metal Hooks): these produced a very large strength increase

compared to the untreated aluminum, even higher than the adhesive reference. This was strongly in contrast with the results obtained using CFRP_1: in order to understand this difference, cross sections of the interface were analyzed. It was possible to see that compared to CFRP_1, with CFRP_2 the Metal Hooks could penetrate the thermoplastic more easily thanks to the different fiber distribution (Fig. 5.20); therefore, they were not damaged during the welding process and the reinforcement was effective, which led to higher shear strengths.

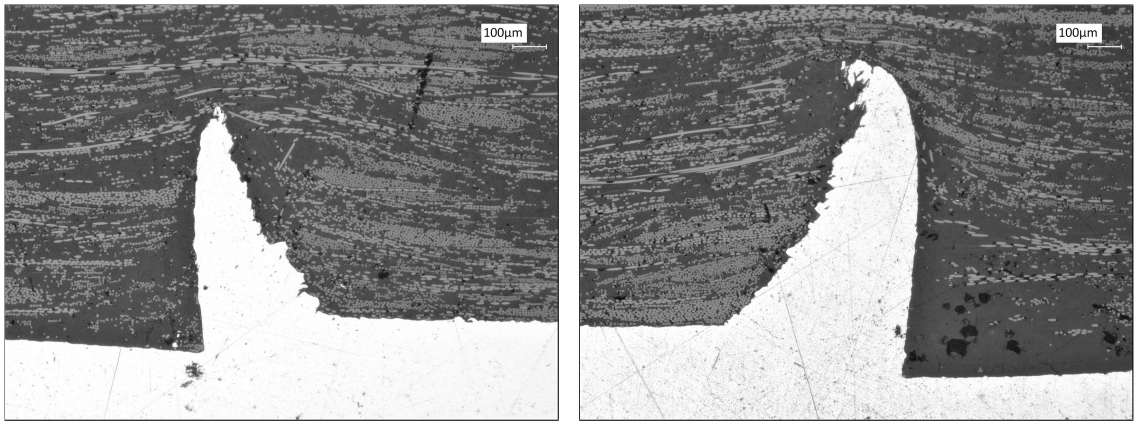

Figure 5.20: *Cross sections of CFRP_2 with Metal Hooks aluminum. Hooks were able to keep their shape and strength after welding*

No big differences were found between the cross sections of CFRP_1 and CFRP_2 with 3D printed pins (Fig. 5.21). Actually, bigger cracks were visible at the base of the pins, even though pin delamination never occurred; however, a large number of fibers could be found on the aluminum after failure (Fig. 5.22), confirming the strengthening effect of the pins. In this case, the pins were probably more effective because they were in contact with a larger number of fibers compared to CFRP_1, which might have increased the amount of load transferred before failure.

Figure 5.21: *Cross sections of CFRP_2 with 3D printed pins.*

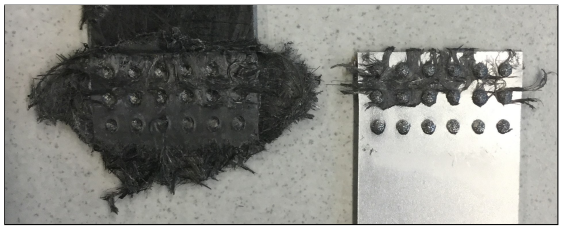

Figure 5.22: *Fracture surfaces of CFRP_2 with 3D printed pins. No energy director was used in this case*

5.3 Conclusion

In this chapter, the differences between several surface pre-treatment were analyzed and discussed in terms of morphology, topography, chemical composition; the effects of the treatments on the joint performance were investigated as well, where it was clear that enhancing mechanical interlocking and surface properties like wettability led to higher strength values.

Laser structuring turned out to be the best treatment using CFRP_1, with strengths comparable to adhesive joints but in much shorter process time; conversion coating treatment was also effective. For all treatments, the first-ply failure area increased with increasing strength, confirming that a stronger adhesion occurred. Through-thickness reinforcements did not produce the desired effects with CFRP_1 but showed to be very effective with CFRP_2, mainly due to the different fiber distribution of the thermoplastic.

Chapter 6

Results: Durability

After investigating the joining process, the adhesion mechanisms and the pre-treatments required to improve the joint performance, the last part of the research focused on assessing how the joint holds out against the effects of moisture and temperature (see Sec. 2.3, 3.2.7). Different pre-treatments of the aluminum were selected: sandblasting, laser and Metal Hooks were chosen among the mechanical treatments, conversion coating among the chemical treatments and plasma for physical treatments. Regarding the thermoplastic, only CFRP_1 was evaluated.

6.1 Moisture Absorption

As explained in Chapter 3, in the first test the main goal was to bring the thermoplastic to moisture saturation and see how the welded area was affected. The test was performed in Toyota (except for the adhesive samples) and the specimens were sent to Delft shortly afterwards. It is relevant to say that an issue occurred during testing: the container where the samples were immersed was not covered, so the water evaporated after a few hours leaving the samples dry for another few hours. Therefore the test was repeated a second time on the same samples, with a cover, and it was successful. This should be taken into account when analyzing the results, since it may have caused an overexposure of the samples. Residual lap shear test was evaluated, as shown in Figure 6.1.

All welded samples showed a decrease in strength depending on the pre-treatments applied. For a clear comparison between the different treatments, the ratio between initial strength and residual strength can be seen in Figure 6.2.

Welds with no treatment or physical treatment (plasma) failed almost immediately; some samples even before testing, with droplets of water visible inside the overlap right after failure.

Differently, mechanical treatments treatments allowed to retain higher strengths, with laser confirmed as the best treatment with 65% of the initial strength; with sandblasting

and Metal Hooks, around 50% of initial strength was obtained. The conversion coating also proved its effectiveness, achieving a residual strength slightly higher than 50% of the original value.

Finally, adhesive samples did not show any strength loss, indicating the sealing effect of the adhesive; actually, with adhesive, higher strengths were obtained after aging, but the samples tested in water were taken from a different batch. Since the application of the adhesive is manual, differences between batches are likely to occur, so it is possible that water was not the cause of the strength increase.

Another observation was related to the scattering of the strength results: for all pre-treatments, a higher scattering after aging can be noticed. It seems that water does not have a homogeneous effect on the welds, with some samples more affected than the others. A significant difference in the power-displacement curves for each treatment was not observed, so the quality of the welds should be similar and not responsible for the higher scattering. However, the reason of this phenomenon could not be further investigated due to shortage of samples at the time of testing.

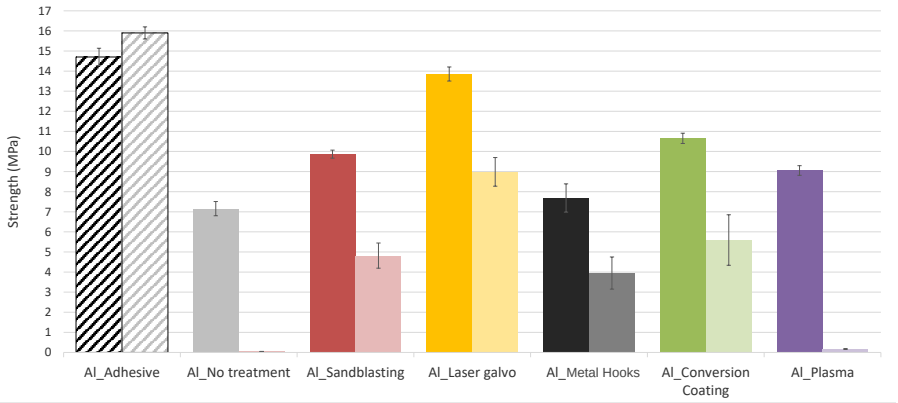

Figure 6.1: *Comparison between lap shear strength before (left columns) and after (right columns) moisture absorption test for different surface pre-treatments.*

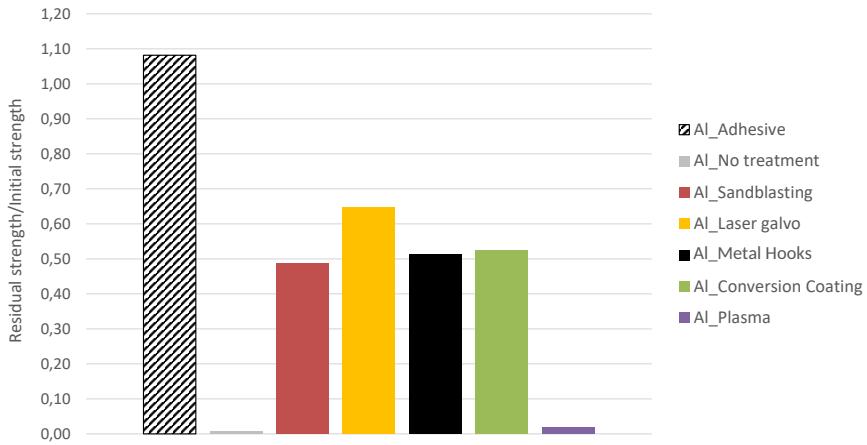

Figure 6.2: *Ratio between initial strength and residual strength after moisture absorption*

Once again, fracture surfaces were analyzed in order to better explain the joint behavior

during artificial aging.

In Figure 6.3, SEM magnifications of the aluminum surface with plasma treatment are shown, and the same characteristics were found on specimens without treatments. It was possible to observe that the whole aluminum surface was deeply altered, indicating that water was able to penetrate everywhere and even to cause deterioration of the aluminum. Therefore, simple plasma was not enough to strengthen the bonds at the interface, which were easily broken by water.

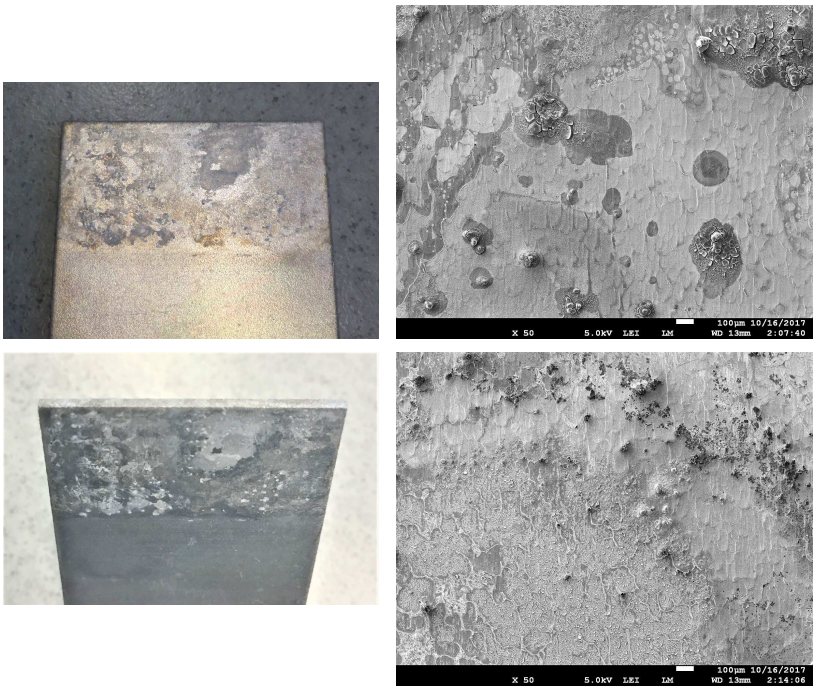

Figure 6.3: *Fracture surface of plasma treated aluminum after artificial aging, inspected both visually and with SEM*

Conversely, with the other treatments the overlap looked quite different. With sandblasting, the edges of the overlap were brownish and looked corroded, but the center was more similar to the original surface, with some resin and fibers still present (Fig. 6.4). This is and indication that the surface roughness was still effective in a portion of the weld.

A similar conclusion could be drawn for laser treated aluminum, which still exhibited quite an amount of resin and fibers inside the grooves, concentrated in the center of the overlap (Fig. 6.5). Since the initial interlocking was stronger than simple sandblasting, the higher residual strength is consistent.

The conversion coated aluminum showed an extremely clean and almost unaffected surface in most of the overlap, with the exception of small portions on the edges (Fig. 6.6). Differently from plasma treatment, the conversion coating might have enhanced the strength of the bonds at the interface, which were able to withstand the effect of water. Besides, it seems that the conversion coating acted as a passivation layer and prevented the water from attacking the aluminum surface, reducing the negative effect of water.

Therefore, it appears that mechanical treatments slowed down water penetration in the overlap by creating some physical barrier, while the conversion coating improved the

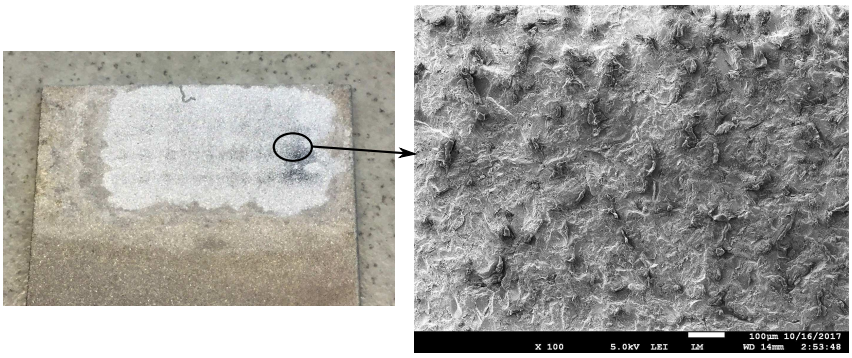

Figure 6.4: *Fracture surface of sandblasted aluminum after artificial aging, inspected both visually and with SEM*

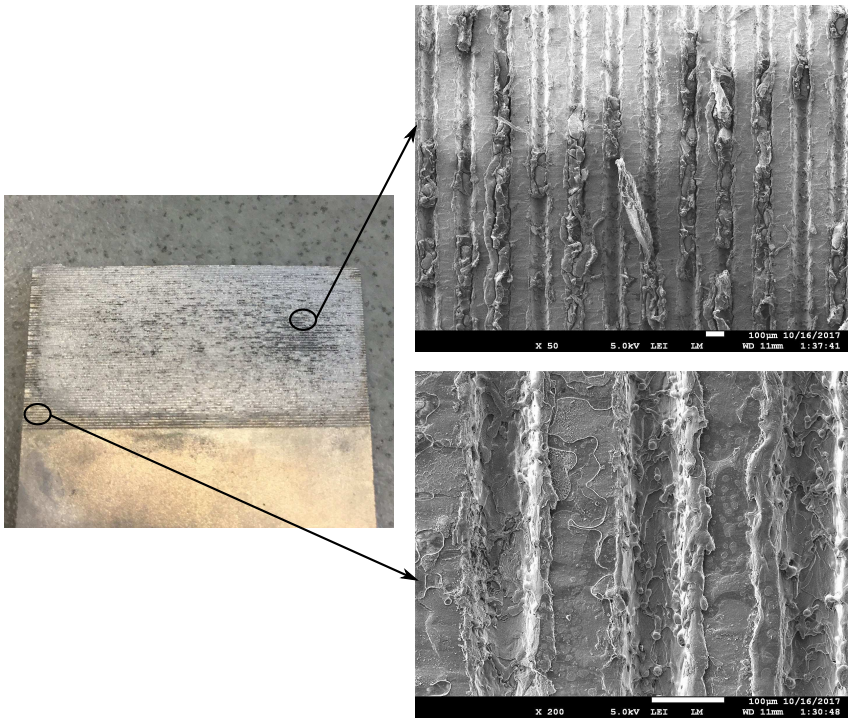

Figure 6.5: *Fracture surface of laser treated aluminum after artificial aging, inspected both visually and with SEM*

corrosion resistance of the weld. However, welds with conversion coating still experienced a significant loss of strength, which might be explained by the small amount of coating (see Sec. 5.1.1), which was not fully effective.

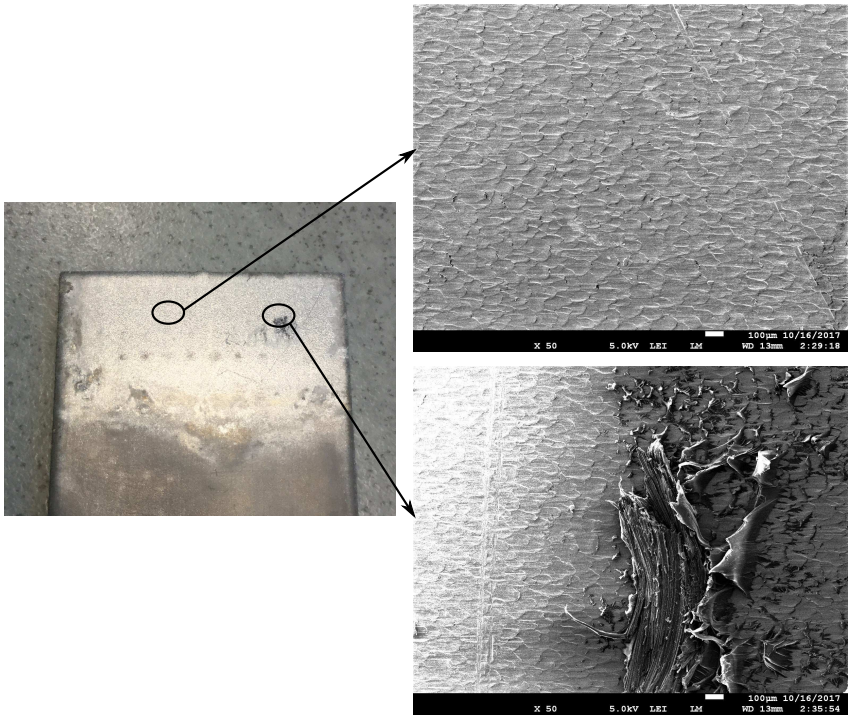

Figure 6.6: *Fracture surface of conversion coating treated aluminum after artificial aging, inspected both visually and with SEM*

6.2 Thermo-humidity Cycle

In the second test, samples experienced humidity for a certain amount of time along with low and high temperatures (Sec. 3.2.7). This test was performed in Toyota as well, while residual strength was evaluated in Delft. Unfortunately, adhesive reference samples could not be aged, but based on the results from the water absorption test, a strength loss due to moisture is not expected. However, the adhesive might be more susceptible to the temperature variation, as well-known from literature [58, 66–68].

Results for residual lap shear strength can be seen in Figure 6.7. Also in this case the ration between initial and retained strength was calculated and shown in Figure 6.8.

Overall, values higher than the moisture absorption test were obtained, but with a similar trend. In terms of absolute value, laser structuring was the best treatment, with strengths around 11 MPa; however, the conversion coating performed slightly better if the relative ratio is considered, with almost 85% of the strength retained.

The other mechanical pre-treatments performed better as well, especially sandblasting, with which it was possible to keep almost 70% of the original strength.

Untreated samples and plasma treated aluminum showed again very poor performances, with only about 20% of the initial strength.

The fracture surfaces of the substrates treated by plasma, sandblasting, laser and conversion coating are shown in Figure 6.9. It is possible to observe that although they look

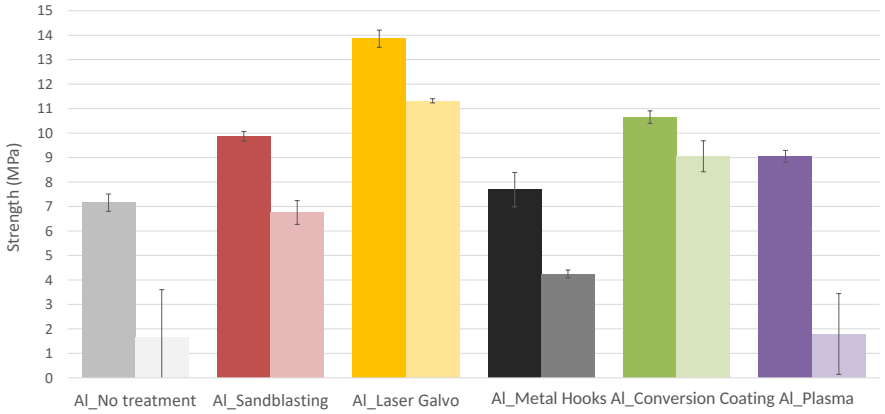

Figure 6.7: *Comparison between lap shear strength before (left columns) and after (right columns) thermo-humidity test for different surface pre-treatments.*

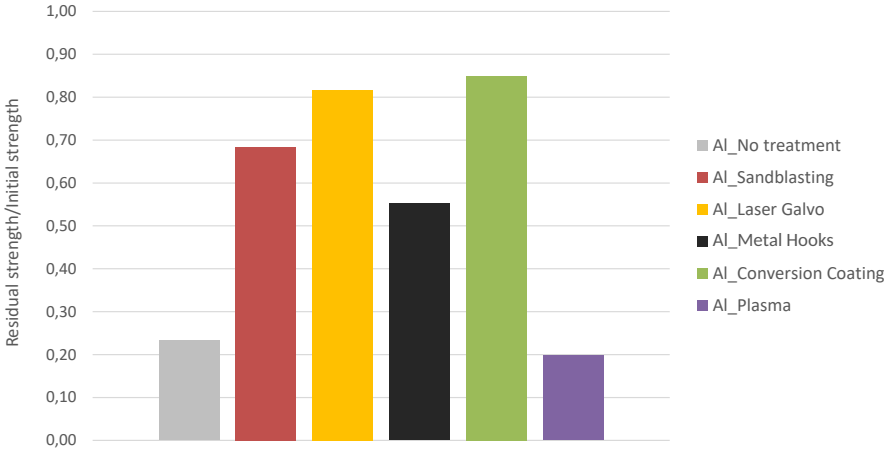

Figure 6.8: *Ratio between initial strength and residual strength after thermo-humidity aging*

much less degraded than after the moisture absorption test, similar characteristics are present after the thermo-humidity cycle.

A considerable amount of fibers and resin can be found in the center of the overlap on the aluminum samples with the best performing treatments, namely laser and conversion coating, followed by sandblasting.

For plasma treated and untreated aluminum samples, almost no mark of the thermoplastic is present, except a small residual of resin on the lower edge of the overlap.

From these results, it seems that moisture and temperature produced results similar to the moisture absorption test, but less detrimental to the substrates or the interface.

Although with a thermo-humidity cycle test it was not possible to identify the separate effects of temperature and moisture, it led to encouraging results because the test was supposed to represent a situation closer to reality. This also gave an indication that the moisture absorption test is very aggressive in terms of water penetration in the joint interface and may overestimate real conditions.

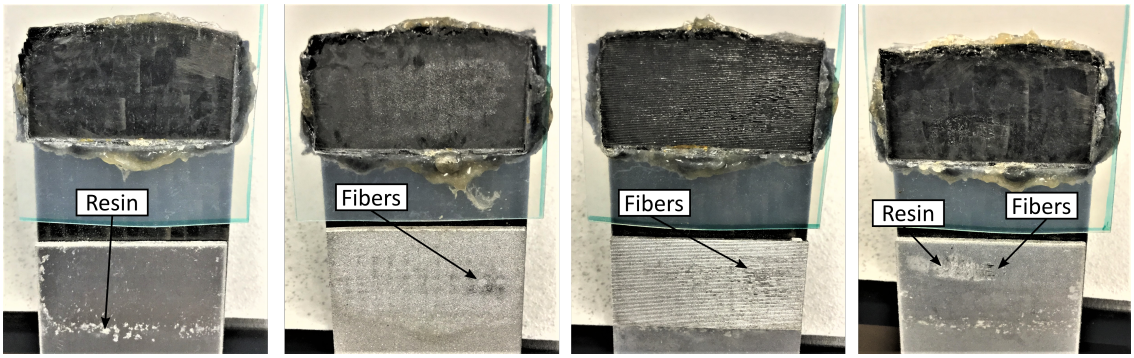

Figure 6.9: *Fracture surfaces after thermo-humidity aging for the different treatments. From left to right: plasma, sandblasting, laser, conversion coating*

6.3 Conclusion

Joint behavior in more aggressive environments after different surface pre-treatments of the aluminum substrate was evaluated. Water (moisture) considerably affects the weld interface, causing a significant loss of adhesion when the aluminum was untreated or treated by only physical methods, such as plasma. The aluminum surface was strongly degraded as well. Other treatments like laser and conversion coating were able to withstand better the environmental effects of moisture.

However, when the joints experienced artificial conditions more similar to reality (a sequence of high and low temperatures, high relative humidity), treated joints could retain up to 85% of the initial strength, showing once again the potential of ultrasonic plastic welding combined with metal surface pre-treamtments.

Chapter 7

Conclusions and Recommendations

7.1 Conclusions

Multi-material joining is considered an important challenge in the automotive industry, with several advanced technologies still in development. In this experimental study, ultrasonic plastic welding was investigated as a candidate technology for direct joining between aluminum and CF/PA6. Since ultrasonic welding is well established for thermoplastic-to-thermoplastic welding, the goal was to analyze the factors affecting adhesion, strength and durability when dissimilar materials were joined together.

An answer to the initial research questions was sought, reaching the following conclusions:

- *What is the melting behavior of the thermoplastic during the welding process and how does it affect the adhesion between CFRP and metal?*

  A successful reference weld was obtained, both using aluminum as top or bottom substrate; the process was confirmed to have good reliability and reproducibility when controlled by sonotrode displacement. It was observed that the main adhesion mechanisms acting during welding were mechanical interlocking of the molten thermoplastic into the aluminum macro and micro-roughness and physical adsorption. Adhesion was found to be stronger close to the metal short edge, where first-ply failure was observed, possibly due to non-uniform temperature distribution; in the rest of the overlap adhesive failure occurred.

- *What is the initial strength of the joint and how does it compare to other joining techniques used in automotive?*

  Lap shear strength was assessed for different weld configurations. It was observed that slightly higher strengths and lower scattering were obtained when aluminum was the bottom substrate with an insulating Kapton film between the metal and the clamping jig. Strengths of 7.16 MPa and 6.94 MPa were obtained with CFRP_1/Al and CFRP_2/Al respectively. These values were quite lower than the strength of adhesive reference joints, indicating that improvements were needed.

- *Based on the adhesion mechanisms, how is it possible to increase joint strength?*

  Different surface pre-treatments on the aluminum substrates were planned, applied and examined to evaluate their effects on the joint performance. Mechanical, chemical and physical treatments were considered: very promising results were obtained using CFRP_1, especially with laser structuring (94% strength increase) and conversion coating (49% strength increase). Strength values were comparable to adhesive joints, but the whole process was much faster even considering the surface pre-treatments.

- *What are the effects of temperature and moisture on adhesion and on the joint performance?*

  After selecting the best aluminum pre-treatments, residual strength of the joints after accelerated artificial aging was evaluated. Penetration of water at the weld interface was recognized to be the main degradation mechanism. Surface pre-treatments showed their potential again by retaining up to 85% of the initial strength after thermo-humidity cycle test. However, untreated samples or physical treatments like plasma showed very poor performance, suggesting that deeper investigation on the weld durability is needed.

The results obtained in this study revealed a new potential of ultrasonic plastic welding to join metals and thermoplastics. This joining technology combined with specific metal surface pre-treatments could lead to important developments in the automotive industry, offering new and valuable solutions in the assembly lines.

7.2 Recommendations

Although knowledge was developed through this study, there is still room for improvement and for new findings. Following research on this topic should focus on:

1. Optimization of the welding process to obtain first-ply failure in the whole overlap
2. Improvement of selected metal surface pre-treatments (laser, conversion coating, chemical plasma), aiming to a better optimization of process parameters
3. Deeper investigation on environmental effects by additional type of tests (i.e. salt spray test, galvanic corrosion, creep)
4. Extension of the study to other material combinations (steel, other thermoplastics)
5. Development of continuous welding

A few simple trials were already explored regarding point 1. Since it was proved that non-uniform adhesion on the overlap is likely due to an irregular temperature distribution, two experiments with untreated aluminum and CFRP_1 were carried out.

In the first one, the energy director was placed only in the "colder" area of the overlap (close to the CFRP short edge) to obtain higher heat generation there. Approximately

one half and one third of the overlap were covered, but in both cases poor bonding was obtained between aluminum and CFRP_1.

In the second trial, welding with higher welding forces and/or amplitudes was tested. In the limits of power generated by the equipment, higher forces mean a reduced welding time, which should correspond to a lower amount of heat dissipated into the aluminum substrate from the interface. Amplitude could be increased because with the aluminum on the bottom, no cracks appeared (differently from what showed in Section 3.2.1, where aluminum was on top). A force of 1500N and amplitude of 34.5 µm was tested, and also 1500N and 43.1 µm. An average lap shear strength of 10.72 MPa with a coefficient of variation of 8.44% was obtained, which is a considerable improvement (+49.72% from the original value) with no surface pre-treatments. Fracture surfaces (Fig. 7.1) presents larger areas of first-ply failure but still not the full overlap. Power-displacement curves can be seen in Figure 7.2, which confirmed the reliability of the process, even with new parameters.

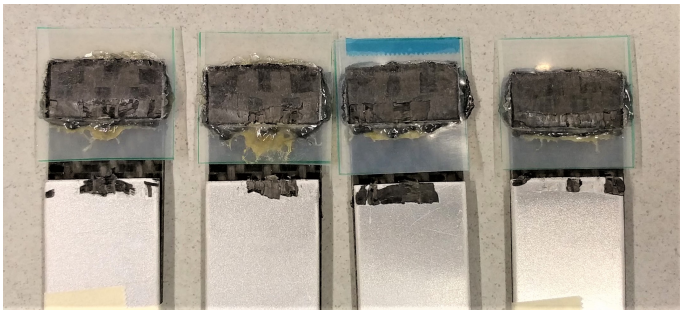

Figure 7.1: *Fracture surfaces of joints welded with the new parameters: 1500N,* 34.5 µm *or* 43.1 µm*, 100% displacement*

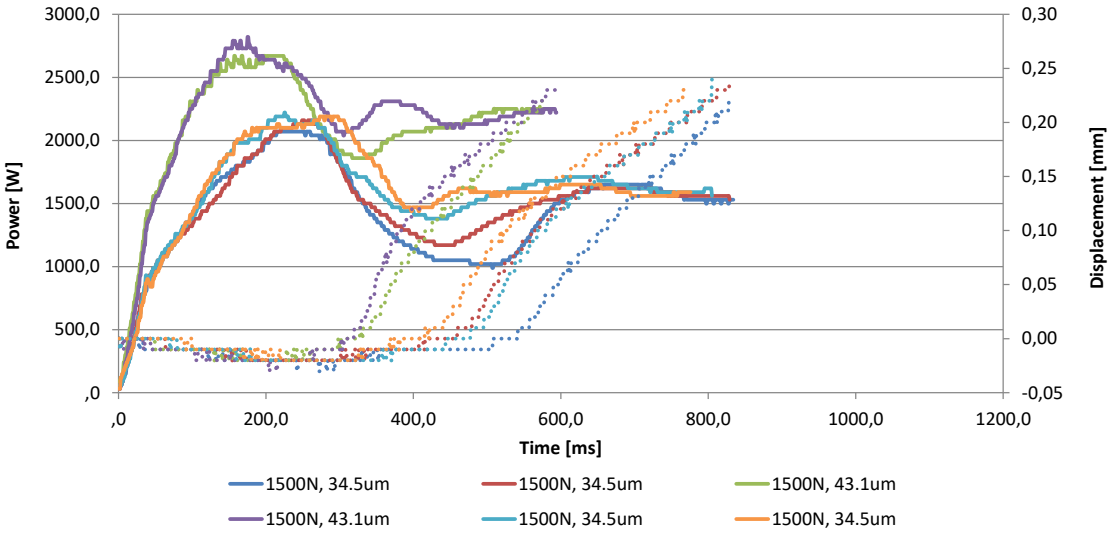

Figure 7.2: *Examples of power displacement curves using higher forces and/or higher amplitudes*

References

[1] Anahi Pereira da Costa, Edson Cocchieri Botelho, Michelle Leali Costa, Nilson Eiji Narita, and José Ricardo Tarpani. A review of welding technologies for thermoplastic composites in aerospace applications. *Journal of Aerospace Technology and Management*, 4(3):255–265, 2012.

[2] Irene Fernandez Villegas, Lars Moser, Ali Yousefpour, Peter Mitschang, and Harald EN Bersee. Process and performance evaluation of ultrasonic, induction and resistance welding of advanced thermoplastic composites. *Journal of Thermoplastic Composite Materials*, 26(8):1007–1024, 2013.

[3] Ali Yousefpour, Mehdi Hojjati, and Jean-Pierre Immarigeon. Fusion bonding/welding of thermoplastic composites. *Journal of Thermoplastic composite materials*, 17(4):303–341, 2004.

[4] A Baldan. Adhesion phenomena in bonded joints. *International Journal of Adhesion and Adhesives*, 38:95–116, 2012.

[5] S Bolt. Ultrasonic plastic welding of carbon fiber reinforced polyamide 6 to aluminium and steel. *TU Delft, Delft University of Technology*, 2014.

[6] SM Goushegir. Friction spot joining (fspj) of aluminum-cfrp hybrid structures. *Welding in the World*, 60(6):1073–1093, 2016.

[7] Christian Lamberti, Tobias Solchenbach, Peter Plapper, and Wulff Possart. Laser assisted joining of hybrid polyamide-aluminum structures. *Physics Procedia*, 56:845–853, 2014.

[8] Guntram Wagner, Frank Balle, and Dietmar Eifler. Ultrasonic welding of aluminum alloys to fiber reinforced polymers. *Advanced Engineering Materials*, 15(9):792–803, 2013.

[9] Irene Fernandez Villegas. In situ monitoring of ultrasonic welding of thermoplastic composites through power and displacement data. *Journal of Thermoplastic Composite Materials*, 28(1):66–85, 2015.

[10] Frank Balle, Guntram Wagner, and Dietmar Eifler. Ultrasonic metal welding of aluminium sheets to carbon fibre reinforced thermoplastic composites. *Advanced Engineering Materials*, 11(1-2):35–39, 2009.

[11] Irene Fernandez Villegas. Strength development versus process data in ultrasonic welding of thermoplastic composites with flat energy directors and its application to the definition of optimum processing parameters. *Composites Part A: Applied Science and Manufacturing*, 65:27–37, 2014.

[12] Christophe Ageorges and Lin Ye. Resistance welding of metal/thermoplastic composite joints. *Journal of Thermoplastic Composite Materials*, 14(6):449–475, 2001.

[13] D Stavrov and HEN Bersee. Resistance welding of thermoplastic composites-an overview. *Composites Part A: Applied Science and Manufacturing*, 36(1):39–54, 2005.

[14] TJ Ahmed, D Stavrov, HEN Bersee, and Adriaan Beukers. Induction welding of thermoplastic compositesan overview. *Composites Part A: Applied Science and Manufacturing*, 37(10):1638–1651, 2006.

[15] Peter Mitschang, Rudi Velthuis, Stefan Emrich, and Michael Kopnarski. Induction heated joining of aluminum and carbon fiber reinforced nylon 66. *Journal of thermoplastic composite materials*, 2009.

[16] Peter Mitschang, Rudi Velthuis, and Mirja Didi. Induction spot welding of metal/cfrpc hybrid joints. *Advanced engineering materials*, 15(9):804–813, 2013.

[17] FC Liu, J Liao, and K Nakata. Joining of metal to plastic using friction lap welding. *Materials & Design (1980-2015)*, 54:236–244, 2014.

[18] YJ Chen, TM Yue, and ZN Guo. A new laser joining technology for direct-bonding of metals and plastics. *Materials & Design*, 110:775–781, 2016.

[19] Kwang-Woon Jung, Yousuke Kawahito, Makoto Takahashi, and Seiji Katayama. Laser direct joining of carbon fiber reinforced plastic to aluminum alloy. *Journal of Laser Applications*, 25(3):032003, 2013.

[20] Seiji Katayama and Yousuke Kawahito. Laser direct joining of metal and plastic. *Scripta Materialia*, 59(12):1247–1250, 2008.

[21] Y Kawahito and S Katayama. Characteristics of lamp joining structures for several materials. In *Proceedings of ICALEO*, pages 1469–1473, 2010.

[22] Yusuke Niwa, Yousuke Kawahito, Shuji Kubota, and Seiji Katayama. Evolution of lamp joining to dissimilar metal welding. In *Proc. ICALEO*, pages 311–317, 2008.

[23] Ren-Yu Yeh and Ray-Quen Hsu. Development of ultrasonic direct joining of thermoplastic to laser structured metal. *International Journal of Adhesion and Adhesives*, 65:28–32, 2016.

[24] Yongrong Wu, Jianping Lin, Blair E Carlson, Peng Lu, Michael P Balogh, Nicholas P Irish, and Yu Mei. Effect of laser ablation surface treatment on performance of adhesive-bonded aluminum alloys. *Surface and Coatings Technology*, 304:340–347, 2016.

[25] Elisabeth Stammen, Klaus Dilger, Stefan Böhm, and Ralf Hose. Surface modification with laser: pretreatment of aluminium alloys for adhesive bonding. *Plasma Processes and Polymers*, 4(S1):S39–S43, 2007.

[26] Adrian S Sabau, Clayton M Greer, Jian Chen, Charles D Warren, and Claus Daniel. Surface characterization of carbon fiber polymer composites and aluminum alloys after laser interference structuring. *JOM*, 68(7):1882–1889, 2016.

[27] Rico Rechner, Irene Jansen, and Eckhard Beyer. Influence on the strength and aging resistance of aluminium joints by laser pre-treatment and surface modification. *International Journal of Adhesion and Adhesives*, 30(7):595–601, 2010.

[28] André Heckert and Michael F Zaeh. Laser surface pre-treatment of aluminum for hybrid joints with glass fiber reinforced thermoplastics. *Journal of Laser Applications*, 27(S2):S29005, 2015.

[29] Wei Xiong, Bamber Blackman, John P Dear, and Xichang Wang. The effect of composite orientation on the mechanical properties of hybrid joints strengthened by surfi-sculpt. *Composite Structures*, 134:587–592, 2015.

[30] S Ucsnik, M Scheerer, S Zaremba, and DH Pahr. Experimental investigation of a novel hybrid metal–composite joining technology. *Composites Part A: Applied Science and Manufacturing*, 41(3):369–374, 2010.

[31] BGI Dance and AL Buxton. An introduction to surfi-sculpt technology–new opportunities, new challenges. In *Proceedings of the 7th International Conference on Beam Technology*, pages 75–84, 2007.

[32] Anita L Buxton and BGI Dance. Surfi-sculpt tm- revolutionary surface processing with an electron beam. In *Surface Engineering; Proceedings of the 4 th International Surface Engineering Congress*, pages 107–110, 2006.

[33] PN Parkes, R Butler, J Meyer, and A de Oliveira. Static strength of metal-composite joints with penetrative reinforcement. *Composite Structures*, 118:250–256, 2014.

[34] EE Feistauer, RPM Guimarães, T Ebel, JF Dos Santos, and ST Amancio-Filho. Ultrasonic joining: A novel direct-assembly technique for metal-composite hybrid structures. *Materials Letters*, 170:1–4, 2016.

[35] DP Graham, A Rezai, D Baker, PA Smith, and JF Watts. A hybrid joining scheme for high strength multi-material joints. In *Proceedings of 18th international conference on composite materials, Jeju, South Korea*, 2011.

[36] Sina Ebnesajjad and Cyrus Ebnesajjad. *Surface treatment of materials for adhesive bonding*. William Andrew, 2013.

[37] European Aluminium Association et al. The aluminium automotive manual. *Joining-Adhesive bonding. EAA*, 2015.

[38] Thomas S Williams, Hang Yu, and Robert F Hicks. Atmospheric pressure plasma activation as a surface pre-treatment for the adhesive bonding of aluminum 2024. *Journal of Adhesion Science and Technology*, 28(7):653–674, 2014.

[39] Kyong Y Rhee, Nak-Sam Choi, and Soo-Jin Park. Effect of plasma treatment of aluminum on the bonding characteristics of aluminum–cfrp composite joints. *Journal of adhesion science and technology*, 16(11):1487–1500, 2002.

[40] Seyed Mohammad Goushegir et al. *Friction spot joining of metal-composite hybrid structures*. PhD thesis, 2015.

[41] Chongchen Xu, Karthik Ramani, and Ganesan Kumar. Thermoplastic adhesive bonding of galvanized steel to polypropylene composite and its durability. *International journal of adhesion and adhesives*, 22(3):187–195, 2002.

[42] MR Bowditch. The durability of adhesive joints in the presence of water. *International Journal of Adhesion and Adhesives*, 16(2):73–79, 1996.

[43] A Baldan. Adhesively-bonded joints in metallic alloys, polymers and composite materials: mechanical and environmental durability performance. *Journal of Materials Science*, 39(15):4729–4797, 2004.

[44] M Grujicic, V Sellappan, MA Omar, Norbert Seyr, Andreas Obieglo, Marc Erdmann, and Jochen Holzleitner. An overview of the polymer-to-metal direct-adhesion hybrid technologies for load-bearing automotive components. *Journal of Materials Processing Technology*, 197(1):363–373, 2008.

[45] DP Graham, A Rezai, D Baker, PA Smith, and JF Watts. The development and scalability of a high strength, damage tolerant, hybrid joining scheme for composite–metal structures. *Composites Part A: Applied Science and Manufacturing*, 64:11–24, 2014.

[46] Mirja Didi, Stefan Emrich, Peter Mitschang, and Michael Kopnarski. Characterization of long-term durability of induction welded aluminum/carbon fiber reinforced polymer-joints. *Advanced Engineering Materials*, 15(9):821–829, 2013.

[47] Sebastian Bremen, Wilhelm Meiners, and Andrei Diatlov. Selective laser melting. *Laser Technik Journal*, 9(2):33–38, 2012.

[48] FJ Monteiro, MA Barbosa, DR Gabe, and DH Ross. Surface pretreatments of aluminium for electroplating. *Surface and Coatings Technology*, 35(3-4):321–331, 1988.

[49] Kazumasa Shimamoto, Yu Sekiguchi, and Chiaki Sato. Effects of surface treatment on the critical energy release rates of welded joints between glass fiber reinforced polypropylene and a metal. *International Journal of Adhesion and Adhesives*, 67: 31–37, 2016.

[50] S Sharifi Golru, MM Attar, and B Ramezanzadeh. Effects of surface treatment of aluminium alloy 1050 on the adhesion and anticorrosion properties of the epoxy coating. *Applied Surface Science*, 345:360–368, 2015.

[51] JH Nordlien, JC Walmsley, H Østerberg, and K Nisancioglu. Formation of a zirconium-titanium based conversion layer on aa 6060 aluminium. *Surface and Coatings Technology*, 153(1):72–78, 2002.

[52] CJ Nonhof and GA Luiten. Estimates for process conditions during the ultrasonic welding of thermoplastics. *Polymer Engineering & Science*, 36(9):1177–1183, 1996.

[53] Arthur Levy, Steven Le Corre, and Irene Fernandez Villegas. Modeling of the heating phenomena in ultrasonic welding of thermoplastic composites with flat energy directors. *Journal of Materials Processing Technology*, 214(7):1361–1371, 2014.

[54] Anthony Kinloch. *Adhesion and adhesives: science and technology*. Springer Science & Business Media, 2012.

[55] Robert D Adams. *Adhesive bonding: science, technology and applications*. Elsevier, 2005.

[56] KJ Kubiak, MCT Wilson, TG Mathia, and Ph Carval. Wettability versus roughness of engineering surfaces. *Wear*, 271(3):523–528, 2011.

[57] Robert N Wenzel. Resistance of solid surfaces to wetting by water. *Industrial & Engineering Chemistry*, 28(8):988–994, 1936.

[58] MD Banea and Lucas FM da Silva. Adhesively bonded joints in composite materials: an overview. *Proceedings of the Institution of Mechanical Engineers, Part L: Journal of Materials: Design and Applications*, 223(1):1–18, 2009.

[59] IU Ojalvo and HL Eidinoff. Bond thickness effects upon stresses in single-lap adhesive joints. *AIAA Journal*, 16(3):204–211, 1978.

[60] AD Crocombe and RD Adams. Influence of the spew fillet and other parameters on the stress distribution in the single lap joint. *The Journal of Adhesion*, 13(2): 141–155, 1981.

[61] L Tong. Bond strength for adhesive-bonded single-lap joints. *Acta Mechanica*, 117 (1):101–113, 1996.

[62] Jungmin Lee and Hyonny Kim. Stress analysis of generally asymmetric single lap adhesively bonded joints. *Journal of Adhesion*, 81(5):443–472, 2005.

[63] WJ Stronge and OER Heimdahl. Stress in single lap joints of dissimilar materials. Technical report, NAVAL WEAPONS CENTER CHINA LAKE CA, 1981.

[64] LC Hollaway. *Handbook of polymer composites for engineers*. Elsevier, 1994.

[65] Andrew D Crocombe and Ian A Ashcroft. Simple lap joint geometry. *Modeling of Adhesively Bonded Joints*, pages 3–23, 2008.

[66] MD Banea and Lucas FM da Silva. The effect of temperature on the mechanical properties of adhesives for the automotive industry. *Proceedings of the Institution of Mechanical Engineers, Part L: Journal of Materials: Design and Applications*, 224 (2):51–62, 2010.

[67] Lucas FM Da Silva and RD Adams. Adhesive joints at high and low temperatures using similar and dissimilar adherends and dual adhesives. *International Journal of Adhesion and Adhesives*, 27(3):216–226, 2007.

[68] RD Adams, J Coppendale, V Mallick, and H Al-Hamdan. The effect of temperature on the strength of adhesive joints. *International Journal of Adhesion and Adhesives*, 12(3):185–190, 1992.

[69] Genevieve Palardy and Irene Fernandez Villegas. On the effect of flat energy directors thickness on heat generation during ultrasonic welding of thermoplastic composites. *Composite Interfaces*, 24(2):203–214, 2017.

Appendix A

Comparison of Energy Directors

Ultrasonic plastic welding requires the use of energy directors to concentrate heat generation at the interface. For this research, initially a 2-layer Ultramid B PA6 film from BASF was used since it was the same used by Bolt [5]. However, welding was never successful in any conditions; when two others PA6 film were tested, welding was always successful. These two films were Akulon F136-E1 (the one chosen for the whole research) and a PA6 film supplied by the Institute for Composite Materials (IVW) of Kaiserslauitern. In order to understand the influence of the energy director in the welding process and why two different results were obtained, Differential Scanning Calorimetry (DSC) and Dynamic Mechanical Analysis (DMA) were carried out to characterize the material properties.

A.1 DSC

A Pyris Sapphire DSC was used as equipment, and 3 runs per sample were performed in order to eliminate the moisture present in the PA6. A heating and cooling rate of 20K/min was chosen for the first two runs and a rate of 10K/min was chosen for the third run. Temperature ranged from -100°C to 300°C with the final cooling until room temperature; 13mg of Ultramid PA6, 14mg of Akulon PA6 and 5mg of Kaiserslautern PA6 were used for the analysis. In Figure A.1, the results of the third run for all the materials is shown. The peaks are different in height due tot he difference in sample mass; however, there is not a clear significant difference in melting and solidification temperatures ($\approx$ 225°C), nor in their glass transition temperatures ($\approx$ 53°C).

A.2 DMA

Since heat generation in ultrasonic plastic welding is proportional to the storage modulus (E') or loss modulus (E'') of the material (Eq. A.1 [5]), DMA was used to obtain these

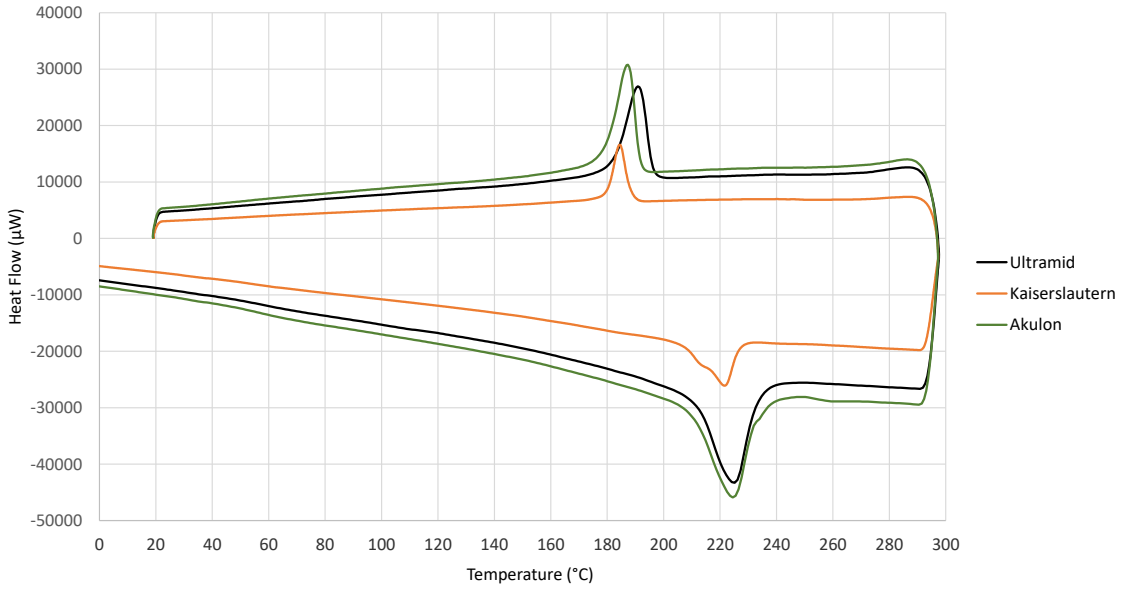

Figure A.1: *DSC of three materials*

values for the Ultramid PA6 and the Akulon PA6. The equipment employed was a Pyris Diamond DMA.

$$\dot{Q} = \frac{\omega \varepsilon^2 E"}{2} \tag{A.1}$$

On the basis of the work of Bolt [5], three frequencies (0.1Hz, 1Hz and 10Hz) were chosen for the test, with a heating rate of 5K/min. The test was carried out from 10°C to 210°C in order to avoid melting of the sample. Results between the three different frequencies were very similar to each other, therefore only 10Hz results are shown in Figures A.2 and A.3. Until 120°C, Ultramid PA6 shows higher storage modulus and until 160°C a slightly higher loss modulus, with a small exception between 55°C and 66°C; looking at the ratio between loss and storage moduli ($tan\delta$, Fig. A.3) the curves for the two materials looks quite similar, without giving any real indication on the difference between them.

In conclusion, from these experiments it was not possible to really determine why one type of PA6 energy director was successful (Akulon) and the other one was not (Ultramid). However, since this was beyond the scope of this research, no further study was conducted and Akulon PA6 was chosen as testing material.

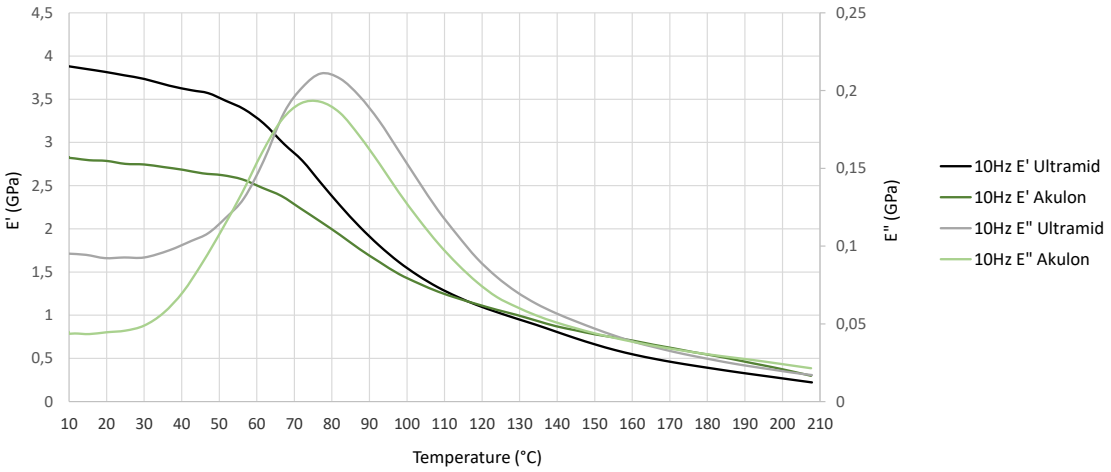

Figure A.2: *Storage and loss modulus versus temperature of Ultramid and Akulon films obtained by DMA analysis*

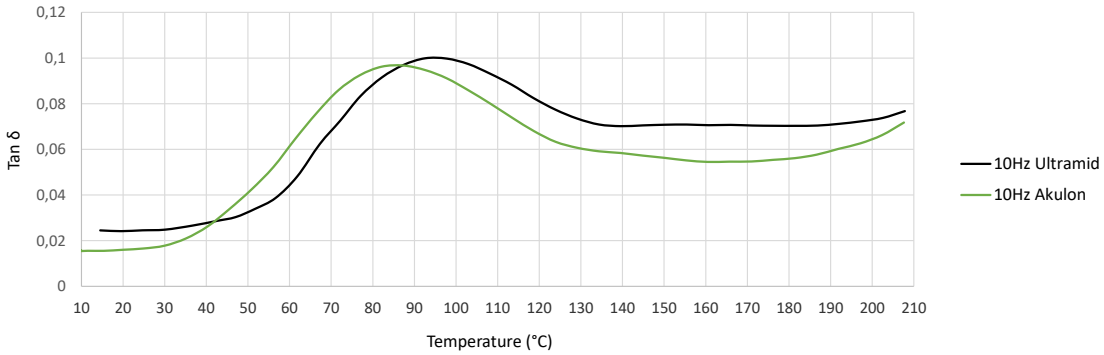

Figure A.3: *Ratio between the loss and the storage modulus (tan δ) versus temperature of Ultramid and Akulon films obtained by DMA analysis*

Appendix B

Welding of Steel

Initially, besides aluminum, CFRP_1 and CFRP_2, also steel was supposed to be included in the research: galvanized advanced high strength dual phase steel was supplied by Toyota Motor Europe. Even if aluminum is the dominant metal for lightweight design, to this day steel has the largest share in automotive manufacturing, therefore it is important to take it into account.

However, with the first welding trials, a few issues arose. First of all, power-displacement curves using steel/CFRP_1 and steel/CFRP_2 (Fig. B.1) were hardly understandable in terms of process monitoring, on the basis of current knowledge on ultrasonic welding [9, 11], no welding stages could be recognized. Besides, from the displacement curve, it was evident that the sonotrode was excessively oscillating: this phenomena is known as hammering and could be detrimental for the equipment.

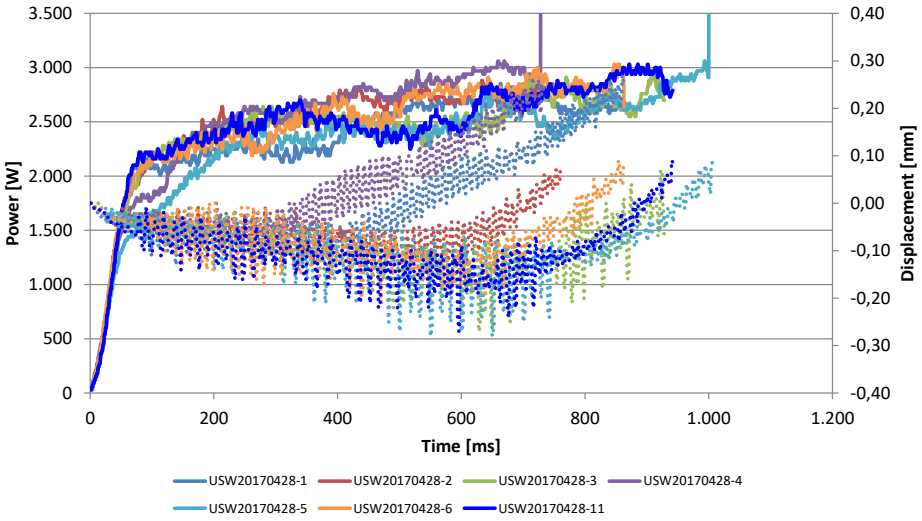

Figure B.1: *Power-displacement curves using steel as top adherend with both CFRP_1 and CFRP_2*

Secondly, using steel as top adherend was damaging the metal surface due to the metal-metal contact with the sonotrode, as explained for aluminum in Section 4.1. However, differently from aluminum, Kapton film was not enough to protect both surfaces, with some resin or film residual always found after welding. Therefore, a serious amount of time was needed for cleaning by scraping the sonotrode, with the risk of damaging its surface. The fact that even Kapton film (which is used to insulate from high temperatures) almost burned (Fig. B.2) shows that very high temperatures are reached in the steel substrate; this could be confirmed also by cross sections, where porosity can be found close to the interface, sign of matrix thermal degradation (Fig. B.3).

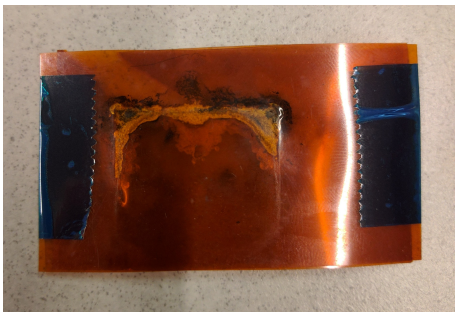

Figure B.2: *Kapton film after welding with steel, where it was placed between the steel substrate and the sonotrode*

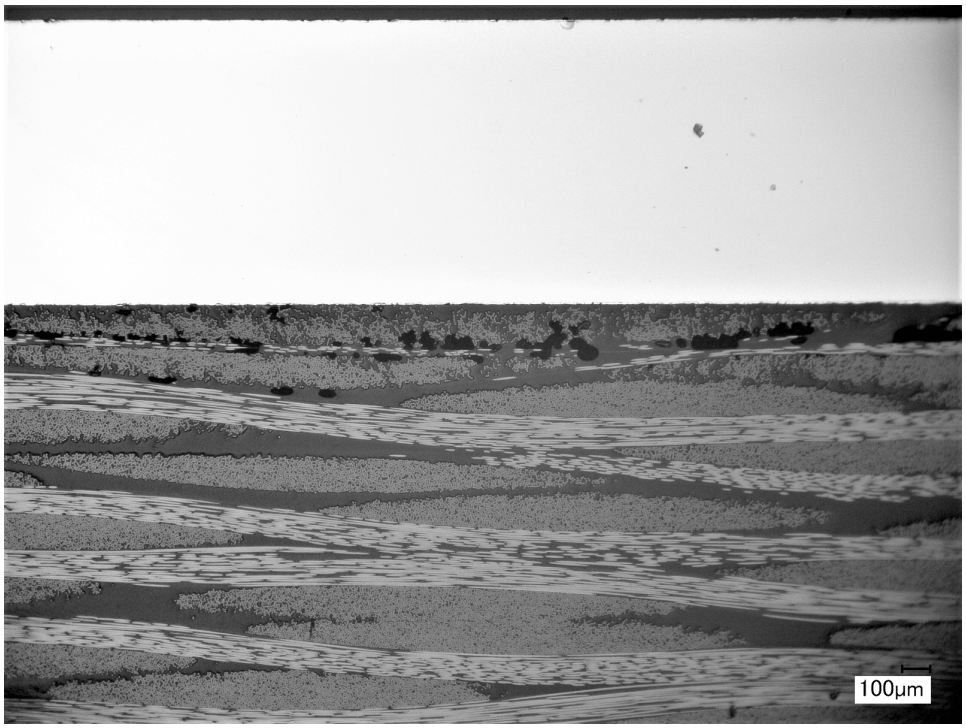

Figure B.3: *Cross section of steel/CFRP_1. Porosity can be seen close to the interface*

Appendix C

Initial Welding Trials

As seen in Chapter 2, the main control parameters in ultrasonic plastic welding are welding force, welding amplitude and sonotrode displacement. The latter can be replaced with energy or time. Besides the values found in literature, some basic trials were conducted to fix the parameters that would be used for almost the whole research. However, many trials initially were not successful due to the Ultramid energy director (see Appendix A), so it is hard to judge weather those settings were good or not. First of all, to have a faster process, high forces and high amplitudes are needed: on the other hand this leads to higher power generation. As shown in Section 3.2.1, semi-amplitued was set at 34.5 µm to avoid cracks in the aluminum. Regarding the force, literature was the main source of information and forces up to 800N were tested; some trials were based on confidential information on values from Toyota Motor Europe as well. Since no significant difference in terms of power-displacement curves was found, eventually the welding force was set to 500N.

Welding both with and without ED were tested; different thicknesses of the ED were used as well, with the results that if the ED is too thin (i.e. 0.09mm), not a good bond was obtained. This is similar to thin ED case with thermoplastic-to-thermoplastic welding [69]. As a consequence, manufacturing of thicker EDs was carried out as explained in Chapter 3. Sonotrode displacement was always set to 100% of ED thickness because it would have been very hard to compare properly the optimum conditions for each surface treatments described in Chapter 3.

Finally, another difference was found between dry and conditioned (before drying) thermoplastics. When conditioned samples were used, clear welding stages typical of ultrasonic plastic welding (Ch. 2.1) were rarely recognizable (Fig. C.1). On the opposite, with dry samples, power-displacement curves with clear power peaks were usually obtained (Fig. C.2).

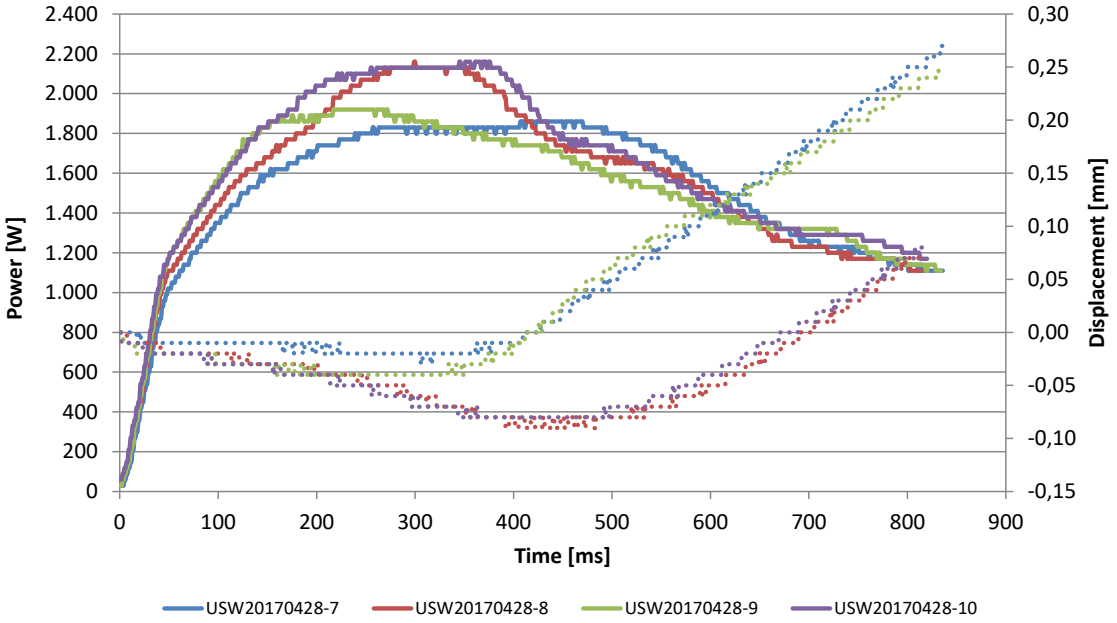

Figure C.1: *Power-displacement curves using conditioned thermoplastics. Welding parameters: 500N, 34.5 µm, 100% ED thickness*

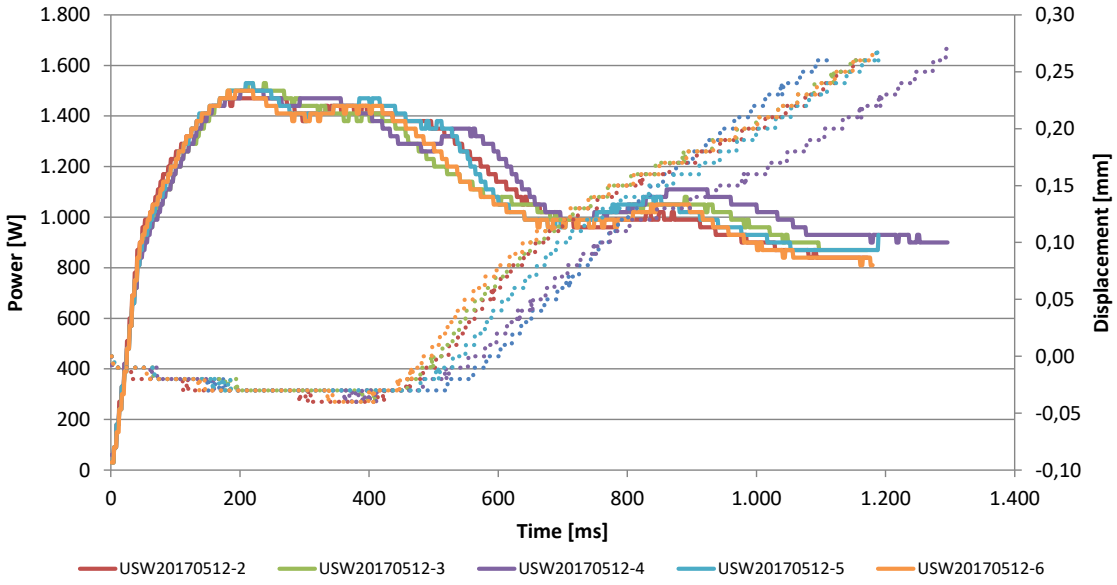

Figure C.2: *Power-displacement curves using dried thermoplastics. Two different power peaks are visible. Welding parameters: 500N, 34.5 µm, 100% ED thickness*

Appendix D

Temperature Measurements

In this appendix, all the measurements carried out to estimate the temperature at the interface are shown.

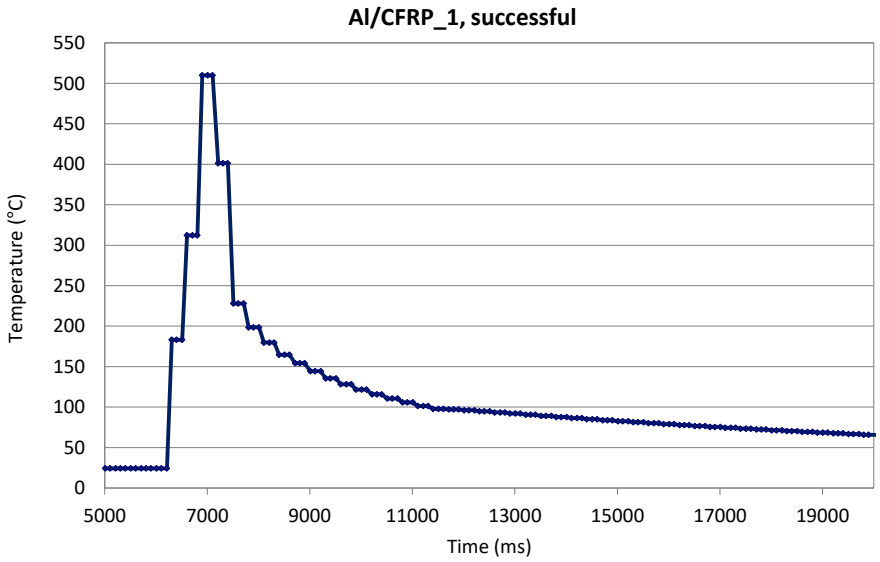

Figure D.1: *Time-temperature curves of the welding process, Al/CFRP_1 configuration, welding successful*

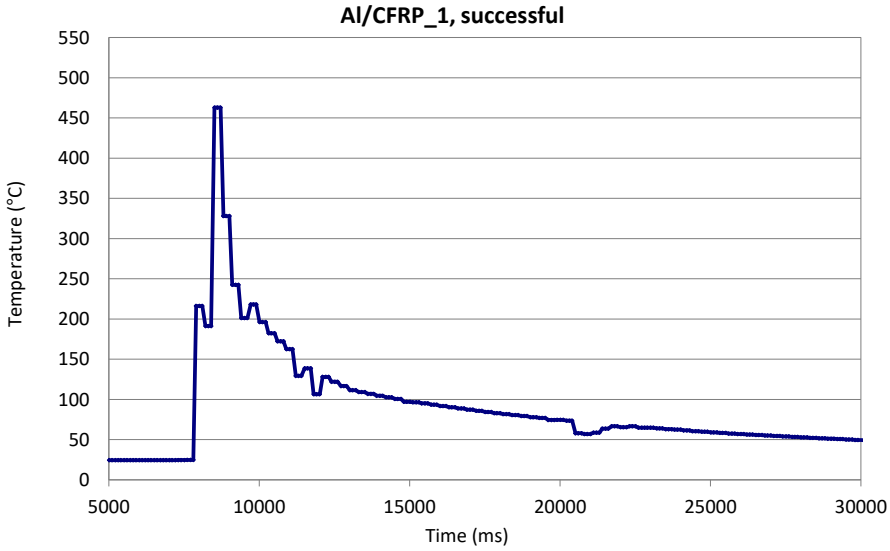

Figure D.2: *Time-temperature curves of the welding process, Al/CFRP_1 configuration, welding successful*

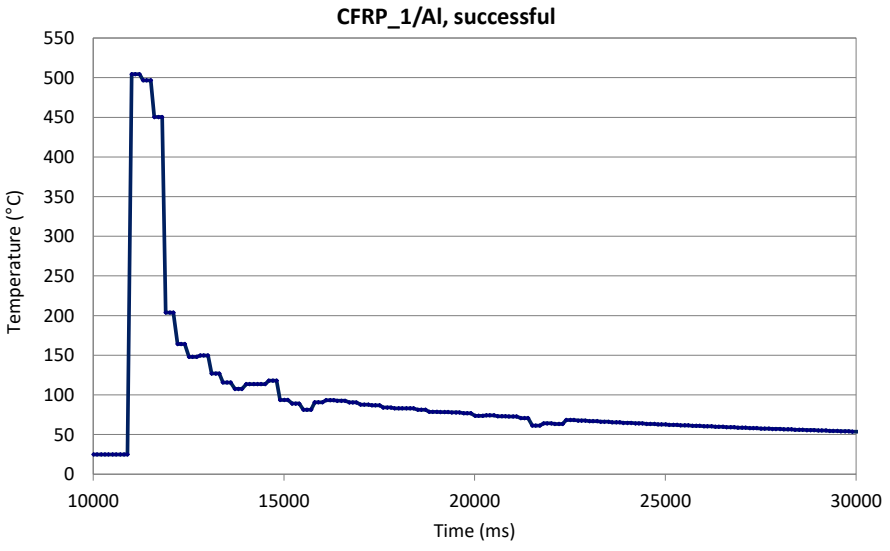

Figure D.3: *Time-temperature curve of the welding process, CFRP_1/Al + Kapton film configuration, welding successful*

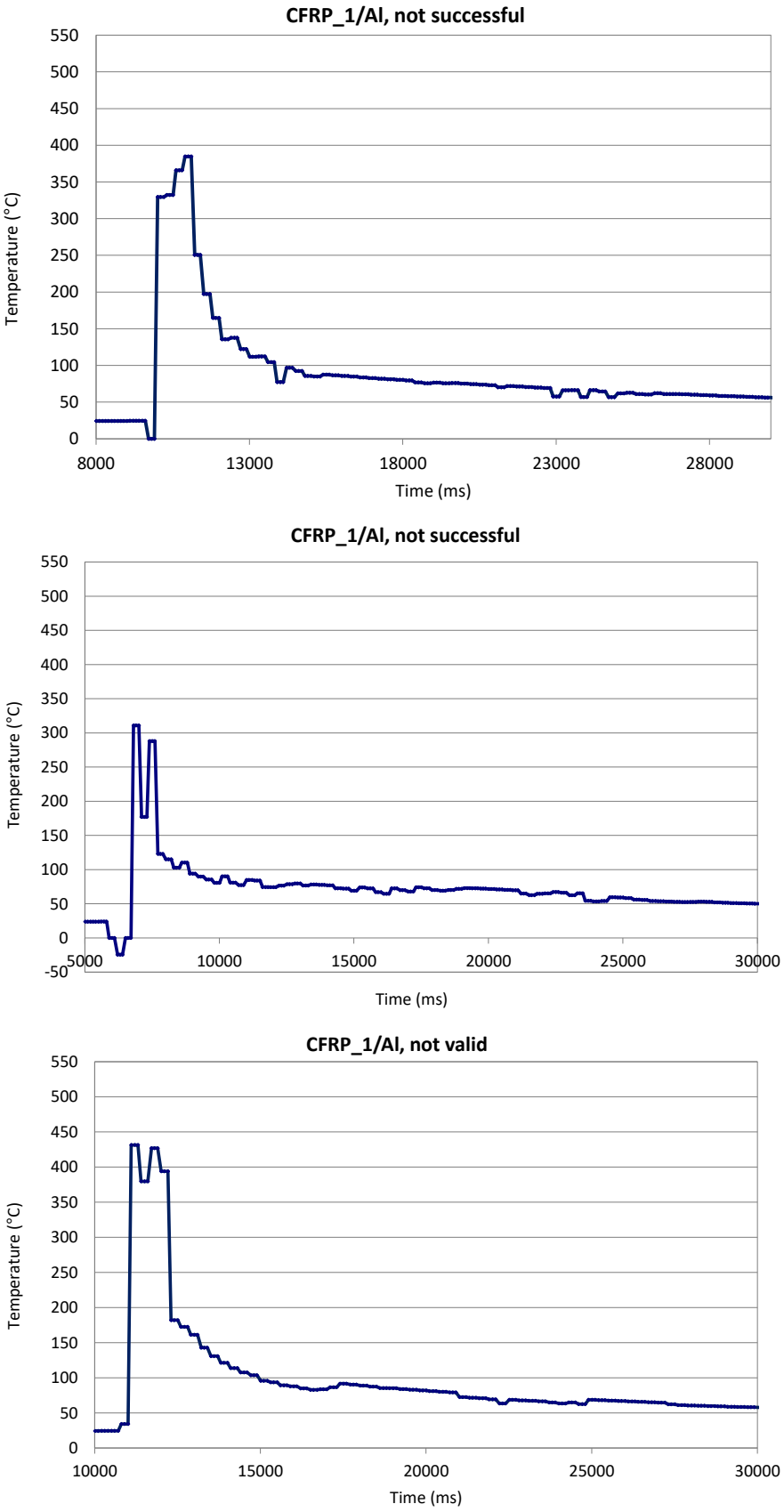

Figure D.4: *Time-temperature curve of the welding process, CFRP_1 /Al configuration, welding not successful*

Appendix E

Cross Sections

In this appendix, the cross sections after treatments which were not discussed in Chapter 5 are presented.

E.1 Conversion Coating

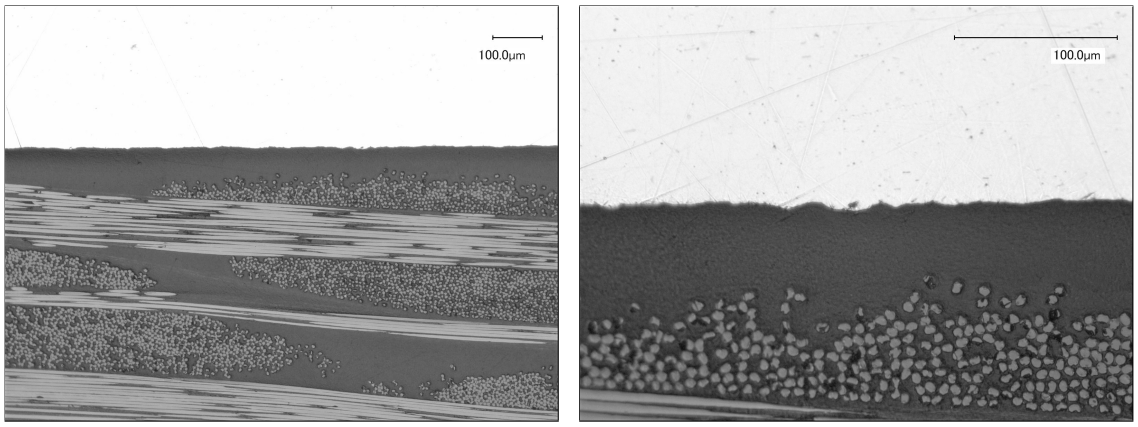

Figure E.1: *Cross sections of a weld with aluminum treated with conversion coating*

E.2 Alkaline-acid Etching

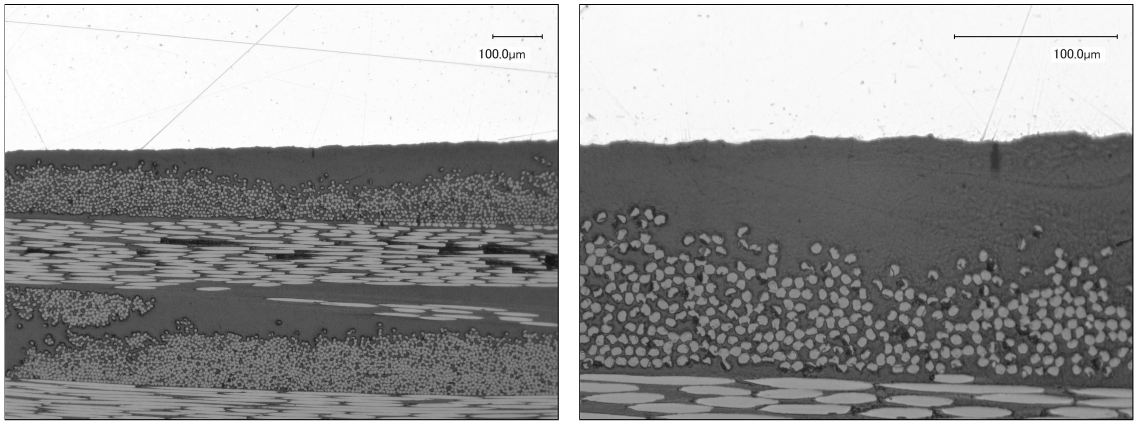

Figure E.2: *Cross sections of a weld with aluminum treated in alkaline and acid solutions*

E.3 Acid Pickling

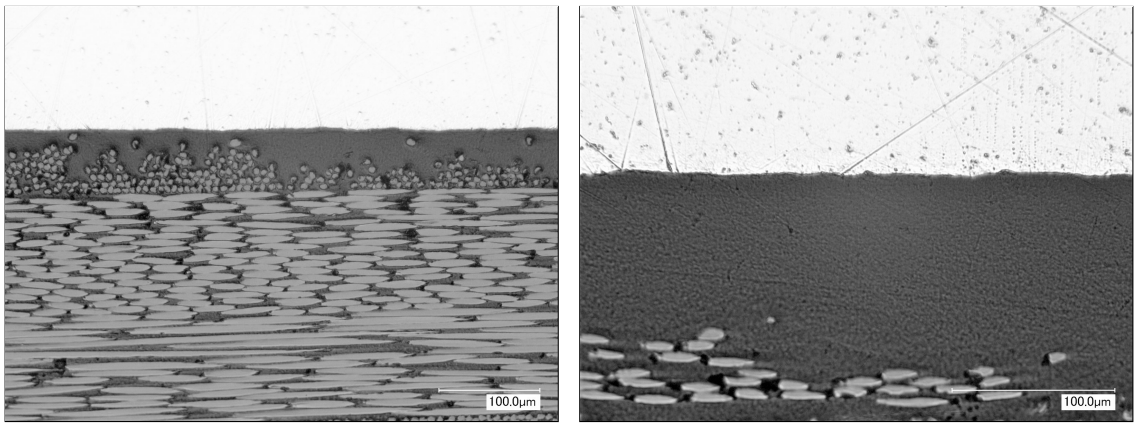

Figure E.3: *Cross sections of a weld with aluminum treated in an acid solution only*

E.4 Plasma

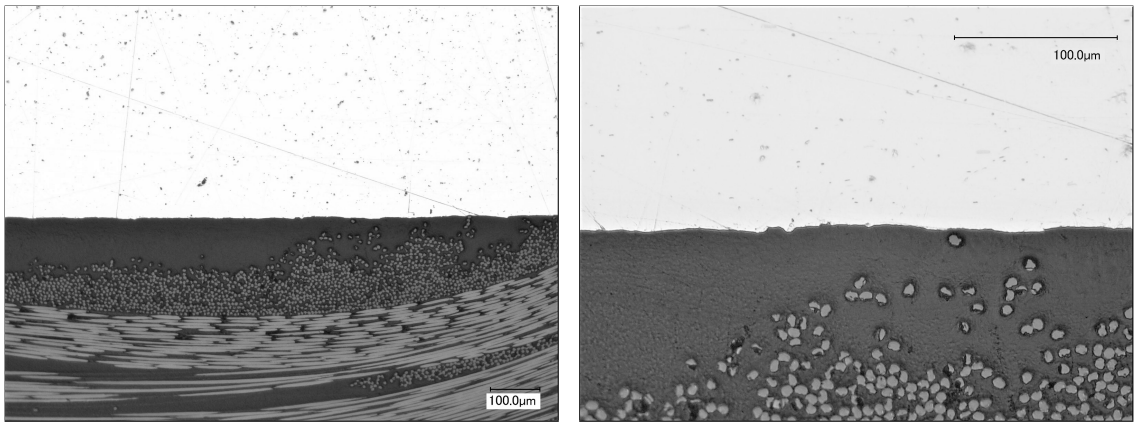

Figure E.4: *Cross sections of a weld with aluminum treated with plasma*